Investigation of second phase concentration effects on tribological and electrical properties of $Cu\text{-}WS_2$ composites

Marco Freschi[1], Matteo Di Virgilio[1,*], Oskari Haiko[2], Marco Mariani[3], Luca Andena[1], Nora Lecis[3], Jukka Kömi[2], Giovanni Dotelli[1]

[1] → Department of Chemistry, Materials and Chemical Engineering "Giulio Natta", Politecnico di Milano, Piazza Leonardo Da Vinci 32, 20133 Milano, Italy

[2] → Materials and Mechanical Engineering, Centre for Advanced Steels Research, University of Oulu, Pentti Kaiteran katu 1, 90570 Oulu, Finland

[3] → Department of Mechanical Engineering, Politecnico di Milano, Via La Masa 1, 20156 Milano, Italy

e-mail addresses: marco.freschi@polimi.it
matteo.divirgilio@polimi.it
oskari.haiko@oulu.fi
marco.mariani@polimi.it
luca.andena@polimi.it
nora.lecis@polimi.it
jukka.komi@oulu.fi
giovanni.dotelli@polimi.it

*Corresponding author: Matteo Di Virgilio, matteo.divirgilio@polimi.it, tel. +39 02 2399 3232

Abstract: In this preliminary study, a set of self-lubricating copper-tungsten disulfide (Cu-WS_2) composites are prepared via a powder metallurgy route to analyze the effects of solid lubricant concentration on their tribological, electrical and wettability properties. An extensive characterization is performed to preliminarily assess the potential application of these metal matrix composites (MMCs) in sliding electrical contacts working under harsh conditions. The experimental results reveal the beneficial effect of WS_2 on the wear behavior of the prepared composites, as demonstrated by friction coefficient, specific wear rate and wear coefficients results. A second phase content in the 10–15 wt % range appears to guarantee the better combination of the desired features.

Keywords: metal matrix composites, solid lubricants, wear mechanism, tribology

1. Introduction

Sliding electrical contacts are electrical junctions between moving (e.g. rotating) and stationary conductors through which power and signals can flow, allowing the continuity of a circuit [1,2]. Regardless of sliding electrical contact configuration, all the assemblies consist of brushes that slip on rings [3]. They are critical components in a wide range of devices, such as commutators for direct current (DC) electromotors in the automotive field, alternators, slip rings for aerospace applications, wind turbines, chip-mounters, micro-computers, and household appliances [4,5].

Copper alloys are used for large current rings, whereas silver and its alloys are preferred when resistance to the formation of hard oxides and to sulfur-containing species is required. Gold or gold alloys are also considered, as they are inert in the atmospheric environment, and they have low catalytic activity in reactions involving organic gases. Generally, silver or gold plating are used as a cladding or electroplate on a bulk metal to reduce the overall cost [5].

Carbon graphite has been historically the primary material employed for brushes, since its crystallographic structure presents weak interlayer van der Waals bonds that encourage lamellar sliding. Electrographite is its direct improvement, in as much it is enriched by a suitable amount of hard particles which assure an acceptable combination between mechanical strength and electrical conductivity. A similar result can be obtained via the combination with metals or resins to give the so-called metal graphite and resin-bonded graphite [4,6]. However, some criticalities arise with carbon-based brushes: the inherently high electrical resistivity, which may implicate an undesired generation of waste heat; the scarce system compliance and lifetime of monolithic members; the limited ability to work with rough rotor surfaces, especially at high speed; the one order of magnitude higher-drop in electrical potential of graphite-metal sliding contacts with respect to metal-metal ones [6]. Furthermore, the overall performance is intimately tied to the friction and wear phenomena occurring at the interface between the two components in contact.

Precious metals, their alloys and copper-based reinforced composites have recently demonstrated worth of further insights for low-voltage and small-current applications due to stable low contact resistance and a reduced wear rate [5]. This last feature becomes imperative for those particular cases in which the reliability of electrical contact must be preserved over long periods, thus limiting required maintenance operations. To further improve the minimization of the wear rate, suitable lubrication is of paramount importance, hence it represents the technical challenge currently addressed by most of the research in this field [7–13].

Solid lubricants technology is rapidly advancing, as they typically own a layered molecular structure of tightly bound atoms that bestows aptitude for sliding and a noteworthy shear resistance. Therefore, they are capable to promote the formation of a thin tribo-film between contacting materials. In such way, optimal low friction and low wear conditions in the specific operating environment can be achieved [8,14]. Graphite, graphene nanoplatelets (GNP) and transition metal dichalcogenides (TMDs) are the primary exponents of these fascinating materials. Two-phase metal matrix composites (MMCs) are typically obtained by coupling a compatible metal matrix, such as copper, with one of these lamellar solids. Conversely, multi-phase MMCs are fabricated by employing two or more different solid lubricants. In both cases, the final array of properties of an MMC blends those of the single phases while conserving their chemical and physical individuality [15]. One of the most widespread techniques to produce MMCs is powder metallurgy (PM), which includes a milling step aimed to favor the solid lubricant's dispersion in the matrix and to discourage unwanted particles' agglomeration.

TMDs are receiving considerable attention as dispersed solid lubricants in MMCs. They are a family of compounds characterized by a general formula TX_2, in which T is a transition metal, such as molybdenum (Mo) or tungsten (W), and X represents a chalcogen, such as sulfur (S), selenium (Se) or tellurium (Te). Amongst them, molybdenum disulfide (MoS_2) and tungsten disulfide (WS_2) are drawing attention to improve the tribological features of particle-reinforced copper-based composites [12,16–20]. They exhibit the typical anisotropic quasi two-dimensional crystal structure of TMDs, comprised of a middle plane of metal atoms sandwiched between two layers of chalcogen atoms [21,22]. The intra-layer bonds are covalent, whereas the inter-layer ones, between adjacent sandwiches, are relatively weak van der Waals forces. Therefore, layers can easily slide when shearing forces are applied. The subsequent generation of a tribo-film on the worn surface, through the continuous supply of lubricant, strongly reduces friction coefficient and wear rate. WS_2 is characterized by chemical inertness, stability to oxidation, powder dispersibility, long service life and an excellent thermal resistance, demonstrated by a 730 °C-maximum operating temperature which is about 100°C higher than that of MoS_2 [16,23]. However, it is more expensive and therefore slightly less competitive than MoS_2 in conventional applications, hence its employment is preferred in those sectors (e.g., aerospace) in which sliding electrical contacts operate under more extreme conditions.

A consistent research effort is being produced to deeply understand and improve the characteristics of copper-tungsten disulfide (Cu-WS_2) composites, with authors focalizing on various parameters of a typical preparation procedure. Zhao et al. [18] have characterized copper-tungsten disulfide composites with variable WS_2 content from 5 to 30 vol %, prepared via spark plasma sintering (SPS), observing a strong improvement in tribological properties. The sample containing 25 vol % of WS_2 has provided the best performance, with a friction coefficient of 0.16 and specific wear rate of 5×10^{-5} mm^3 N^{-1} m^{-1}. The authors have verified the formation of an overall 60 nm-thick tribo-film composed of a thinner oxygen-rich layer and a thicker copper sulfide (Cu_2S)-rich one, whose presence has directly affected the friction and wear behavior by impeding the contact between studied composites and the counter ball during wear tests. Xiao et al. [19] have fabricated Cu-WS_2 composites with a solid lubricant's content up to 40 vol % by hot-pressing (HP). Tribological testing has allowed to monitor a remarkable reduction of the friction coefficient and to identify delamination wear as the main wear mechanism, with WS_2 layers arranging horizontally in the tribo-film. Differently from other species such as graphite [24], Cu-WS_2 composites have revealed a higher Vickers hardness (up to 94.7 HV) than pure copper (75.4 HV). The annealing of the samples at different temperatures from 700 to 950 °C has demonstrated a progressive accentuation of the decomposition of tungsten disulfide and the undesired formation of Cu_2S, with a consequent worsening of the tribological performance. Zhou et al. [20] have analyzed the effect of different grain sizes (0.6 and 5.0 μm) of WS_2 particles on the mechanical and tribological properties of Cu-WS_2 composites with a 20 wt %-content of lubricating phase. Although both composites have showed self-lubricating properties, the specimen containing larger particles has displayed higher bending strength (292.2 vs 181.5 MPa), higher Brinell hardness (96.3 vs 91.1 HB), lower friction coefficient (0.158 vs 0.172) and lower wear rate (2.99×10^{-5} vs 6.13×10^{-5} $mm^3 N^{-1} m^{-1}$). This discrepancy has been attributed to the higher bonding strength that larger WS_2 particles exhibit with the copper matrix, able to favor the generation and a longer propagation of microcracks at the phase interface. Moreover, the smoother transfer film, the lower concentration of tribo-oxidation products and the smaller wear debris observed in the composite with 5.0 µm WS_2 particles have contributed to its better wear resistance. Wang et al. [25] have reported differences in friction coefficient of Cu-WS_2 composites depending on the production method: samples manufactured through HP have displayed an approximately halved friction coefficient (≈ 0.20) with respect to samples prepared via SPS (≈ 0.40). Concerning hardness and wear rate, values of the same order have been measured regardless of the exploited technique.

This work aspires to investigate the effects of a fundamental aspect of the preparation of self-lubricating Cu-WS_2 tablets, namely the tungsten disulfide content. From previous studies of our research group [26], promising results have been obtained for a 10 wt %-concentration of WS_2. Therefore, a set of composites with progressive 5 wt %-increase in WS_2 content ranging from 5 wt % to 30 wt % has been prepared while considering the one connoted by a 10 wt % of WS_2 as a benchmark. PM has been selected as the most reliable production technique, as it combines affordability and process simplicity. Firstly, the ball milling step has been executed to properly mix, grind, and homogenize the metal matrix and the solid lubricant powders. Then, powder compaction and tableting has been achieved via cold pressing. In the end, solid-state pressureless sintering has allowed to further increase density and mechanical strength of the manufactured tablets. Granulometry tests, X-ray diffraction (XRD), Raman scattering spectroscopy, static optical contact angle (OCA) measurements, scanning electron microscopy (SEM), density evaluation, electrical properties assessment, indentation hardness tests, micro-scratch tests, wear tests and laser confocal scanning microscopy have been exploited to perform an extensive characterization of the prepared samples, in order to ascertain their electrical, mechanical and tribological properties and, consequently, their potential practicability in sliding electrical contacts working under harsh conditions.

2. Materials and Methods

2.1 Materials

Electrolytic copper powders with a nominal particle size of 45 μm and a purity level > 99.5% have been acquired from Makin Metal Powders (Rochdale, UK). Sigma-Aldrich Corporation (St. Louis, MO, USA) has supplied tungsten disulfide micro-powders with a mean particle size of 2 μm and a purity of 99%. Following the procedure employed by the authors in [26], copper powders have been initially dried in oven (G-2100, F.LLI GALLI G. & P. snc, Fizzonasco di Pieve Emanuele, Italy) at 120 °C for 6 hours to remove residual moisture. A 1-level roller ball milling system (MGS S.r.l., Olginate, Italy) has been employed to mix and grind Cu and WS_2 powders, in order to obtain a homogenous dispersion with smaller particles. Powders have been placed inside a polyethylene (PE) container together with 15-mm diameter zirconia (ZrO_2) spheres with a 10-to-1 ball-to-powder weight ratio (BPR). The container has been in turn inserted in a cylindrical porcelain alumina jar, which has been rolled on the mill at 60 rpm for 2 hours. Powder compaction and tableting has been achieved via cold-pressing: 1.5 g of milled powder have been introduced into a steel tablet-making device and subjected to a 6 tons-pressure for five minutes by means of hydraulic press (Specac Ltd., Orpington, UK), to obtain tablets characterized by a 13 mm-diameter and a thickness of roughly 2 mm. Afterwards, samples have undergone a sintering process in a EHA Model 1200 °C E-Range Tube Furnace (Carbolite Gero Ltd., Hope, UK) equipped with a thermocouple, to check the temperature of the 6 cm-diameter ceramic inner tube, and two Brooks® Instrument (Hatfield, PA, USA) Smart Mass Flow Controller 5850, to guarantee a flow atmosphere of 95% N_2 and 5% H_2. A heating rate of 8 °C min^{-1} has been applied up to a temperature of 550 °C, which has been maintained for one hour. This specific value has been chosen to avoid thermal decomposition of the lubricating agent, determined from previous thermogravimetric analyses on pure WS_2 powders. In the end, the treated tablets have been naturally cooled down in the process environment.

This procedure has been employed to fabricate a set of five self-lubricating composites with WS_2 concentrations of 5, 15, 20, 25 and 30 wt %. The main difference with the experimental setup proposed by Xiao et al. [19] is the sintering process. The use of cold pressing, the heating rate (8 °C min^{-1}), the operative temperature (550 °C), and the holding time (1 hour) selected in this work aim to limit the formation of unwanted Cu_2S traces, which have been detected in [19], because they are detrimental from a tribological point of view and worsen the overall electrical conductivity.

The samples have been denominated Cu-XWS_2, in which X represents the lubricant mass content. Furthermore, the promising composite with 10 wt %-content of WS_2, previously investigated by our research group [26], has been considered as a benchmark and subjected to additional analyses to perform a complete comparison and to better understand the effects of the second phase content on the features of copper matrix composites. Due to the commonality of the raw materials batches and to be consistent with the above-mentioned designation, the benchmark sample has been recognized as Cu-10WS_2.

2.2 Granulometry tests

Granulometry tests have been performed on the milled powders by means of the Particle Size Analyzer CILAS 1180 L (CILAS SA, Orléans, France), which combines laser diffraction with a CCD camera to measure both fine and coarse particles in the dimensional range between 0.04 and 2500 µm.

2.3 X-ray diffraction analysis

X-ray diffraction (XRD) has been executed via the diffractometer D8 Advance (Bruker Corporation, Billerica, MA, USA), by employing a Cu-Kα filament to emit X-rays with a wavelength of 1.54 Å. A scanning rate of 0.02° per second in the angular interval of 5–90°, an applied tension of 40 kV, an applied current of 40 mA and a count time of one second have been set up as operating parameters during the experiments.

2.4 Raman scattering spectroscopy

Raman scattering spectra have been acquired by means of the Jobin Yvon LabRAM HR800 Raman spectrometer (HORIBA, Kyoto, Japan), which was paired with a 50x objective-microscope model BX41 (Olympus Corporation, Tokyo, Japan). Three acquisitions of 20 seconds have been performed for each sample by applying an excitation via a solid-state neodymium-yttrium aluminum garnet (Nd:YAG) laser (wavelength of 532 nm) at a power of 5 mW.

2.5 Optical contact angle measurements

The OCA 15plus (DataPhysics Instruments GmbH, Filderstadt, Germany), equipped with a 752x582 pixels-resolution CCD video-camera and supported by the image processing software SCA 20, has allowed to obtain static optical contact angle (OCA) measurements via a sessile drop method.

2.6 Scanning electron microscopy

The scanning electron microscope model Stereoscan 360 (Cambridge Scientific Instrument Company, London, UK) has been used to acquire micrographs of the samples polished cross-sections at 500x, 1000x and 3000x magnifications.

2.7 Density measurements

Density assessments have required the hydrostatic balance YDK01 (Sartorius AG, Göttingen, Germany), which enables to weigh the specimens both in air and in water. Absolute density of the composites, identified as δ (g cm^{-3}), has been derived exploiting the Archimedes' principle through Eq. (1):

$$\delta = \frac{m_a \, \delta_w}{m_a - m_w} \tag{1}$$

in which m_a is the mass in air (g), δ_w is the density of water (g cm^{-3}) and m_w is the mass of the solid completely immersed in the solvent (g). Considering the tabulated density of pure copper (δ_{Cu}), equal to 8.96 g cm^{-3} [27], the corresponding relative densities (δ_r, %) of the samples have been determined via Eq. (2):

$$\delta_r = 100\frac{\delta}{\delta_{Cu}} \quad (2)$$

2.8 Electrical properties evaluation

The DC resistance-meter model 2841 (B&K Precision Corporation, Yorba Linda, CA, USA) has been employed to measure the electrical resistance of each composite. The dependence of the resistance values to the geometrical conformation of the analyzed samples has been minimized by exploiting two different measurement configurations. In the first one, test clips have been positioned at the edges of the tablet to maximize their distance. The second one has been attained by shifting one clip towards the central section of the specimen. The corresponding electrical resistivity ρ (Ω m) has been calculated through the second Ohm's law, reported in Eq. (3), in which R is the surveyed resistance (Ω), t is the thickness of the tablet (m), l is the length (m) of the chord perpendicular to the inter-distance, d (m), and placed halfway between the two clips (Fig. 1):

$$\rho = \frac{R\,t\,l}{d} \quad (3)$$

The geometrical parameters have been manually assessed with a Fujisan digital micrometer.

2.9 Scratch tests

Micro-scratch tests have been executed by means of the Micro-Scratch Tester MST 06-0222 provided by CSM Instruments (now Anton Paar TriTec SA, Corcelles, Switzerland). It is equipped with a conical Rockwell stainless steel indenter with a 200 µm-radius spherical diamond tip. A pre-scan and a post-scan stage have been performed with the lowest normal load (0.03 N) to correct measurements for the initial profile and measure the residual depth (R_d, mm) after scratching. The actual scratch stage has been completed by applying a normal load (F_n) of 15 N at a constant speed of 20 mm min^{-1} for a length l_s equal to 3 mm, in order to record the evolution of the tangential force (F_t, N) and the penetration depth (P_d, mm). A minimum of six suitable measurements for each specimen has been extrapolated from a set of ten scratches by discarding outliers. The parameters directly acquired from the experiments have enabled the evaluation of the apparent friction coefficient (*FC*), scratch hardness (H_s, MPa) and degree of penetration (*DoP*) values. Friction coefficient has been computed through Eq. (4) as the ratio between the actual tangential force and the actual normal force:

$$FC = \frac{F_t}{F_n} \tag{4}$$

FC values so calculated combine two different components, originated by adhesion and deformation [28]; the deformation component can be quite high in scratch tests, therefore *FC* values cannot be directly compared with friction measurements performed during wear testing (in which tribo-film formation can also play a dominant role).

Eq. (5) has allowed to estimate scratch hardness as the ratio between the actual normal force and the normally projected contact area (A_c, mm^2) [29,30]:

$$H_s = \frac{F_n}{A_c} \tag{5}$$

Considering the indenter's spherical tip, contact area has been assumed as that of a half circle [31], whose contact radius has been evaluated from the geometry of the tip and the penetration depth.

Degree of penetration has been evaluated from Eq. 6 as the ratio between P_d and half of the contact area width (*w*, mm) [32]:

$$DoP = \frac{P_d}{w} \tag{6}$$

2.10 Indentation hardness tests

Indentation hardness tests have been carried out through the Microhardness Tester FM700 (TECMET 2000 S.r.l., Corsico, Italy). The instrument includes a square based pyramid as indenter, characterized by an angle (θ) of 136° between the opposite faces of the pyramid. Eq. (7) has permitted the computation of Vickers hardness (*HV*) values as average of three different estimations recorded on the upper, central, and lower sections of the tablet:

$$HV = \frac{2P\ \sin\left(\frac{\theta}{2}\right)}{L^2} \tag{7}$$

where P is the applied load of 4.9 N and L is the average length (mm) of the diagonal left by the indenter on the samples.

2.11 Wear tests

Wear tests have been conducted by means of a CSM Instruments (now Anton Paar TriTec SA, Corcelles, Switzerland) tribometer, implementing a ball-on-disk configuration. Both the sample and the counter ball have been preliminarily blown using compressed air before each experiment. A 100Cr6 steel counter ball, connoted by a diameter of 6 mm and a hardness of 831±21 HV, has been selected to effectively probe the softer copper-based composites without excessively deform or crash them. The normal load (F_n) acting on the ball has been fixed to 5 N. The tablets have been fastened to a mandrel and rotated at a controlled tangential speed of 0.18 m s^{-1}. The counter ball has been locked in its ball holder to avoid rolling. In such way, it has slid on the composites producing a circular trail of radius 4.5 mm by covering an overall sliding distance (d) of 500 m. Each test has been made under room temperature and atmosphere. The evolution of the prepared materials' friction coefficient has been considered as a function of the covered distance to infer their wear behavior. The optical microscope (OM) Eclipse LV150NL (Nikon, Tokyo, Japan) has allowed to examine the wear tracks of the composites at 25x and 50x magnifications. The scanning electron microscope EVO 50 EP/LZ4 PENTAFET (Carl Zeiss S.p.A., Oberkochen, Germany) has been chosen to check the wear tracks' surfaces at 400x and 1500x magnifications and the corresponding cross-sections at 20000x magnification.

2.12 Laser confocal scanning microscopy

The laser confocal scanning microscope model VK-X200 by Keyence Corporation, Osaka, Japan, has been employed to inspect the specimens subjected to scratch and wear tests, with the aim of appraising their morphology and wear deformation. Prior to the analysis, the samples have been blown using compressed air to remove coarse debris on their surfaces. The software VK Analyzer Plus has permitted the geometrical inspection of the wear groove and the residual material plastically displaced at the edges in ten different sections of the track for each specimen, as reported in Fig. 2. Volumetric wear losses W_v (mm^3) have been computed via Eq. (8) [32,33]:

$$W_v = (A_g - A_{dm})\, l \tag{8}$$

In both equations, A_g and A_{dm} correspond to the cross-sectional area (mm^2) of the groove and of the total displaced material, respectively. The length l (mm) represents scratch length l_s for the scratches, and the track circumference C for the wear tracks. The corresponding specific wear rates W ($mm^3\ N^{-1}\ m^{-1}$) have been obtained (Eq. (9)) dividing the volumetric losses by the specific sliding distance s_d (m), 0.003 m for scratch tests and 500 m for wear tests, and the applied normal load F_n (N), 15 N for scratch tests and 5 N for wear tests:

$$W = \frac{W_v}{s_d\, F_n} \tag{9}$$

The Archard model can be expressed through Eq. (10) [34,35]:

$$\frac{W_v}{s_d\, F_n} = \frac{k}{H} \tag{10}$$

in which H (MPa) is scratch hardness (H_s) and Vickers hardness (HV) for scratch and wear tests, respectively, whereas k is the dimensionless wear coefficient. This parameter has been directly estimated for both scratch tests and wear tests combining Eq. (8), Eq. (9), and Eq. (10) to obtain Eq. (11):

$$k = \frac{(A_g - A_{dm})\, l\, H}{s_d\, F_n} \tag{11}$$

3. Results and discussion

3.1 Granulometry

Fig. 3 displays the particle size distributions of Cu and Cu-XWS_2 powders. The distribution curves are rather broad, indicating an effective mixing and grinding process [36,37]. Nonetheless, some differences can be spotted with the increase of lubricant amount. Similar to Cu-10WS_2, Cu-5WS_2 and Cu-15WS_2 show narrower monomodal distributions with a modal diameter of 15, 16 and 17 µm respectively. Cu-20WS_2 reports a slight increase in distribution width and a tendency towards bimodality, as the main contributions are represented by particles with diameters of 8 and 17 µm. This behavior is further emphasized in Cu-25WS_2 and Cu-30WS_2, whose distributions are characterized by an increase of particles with similar dimension in the 8–17 µm range. The increase of solid lubricant content determines a more pronounced presence of particles with diameter close to 0.6 µm.

3.2 X-ray diffraction

X-ray diffraction (XRD) patterns of the Cu-XWS_2 composites are highlighted in Fig. 4. Typical copper peaks can be noticed at about 43° for Cu (1 1 1), at about 51° for Cu (2 0 0) and at about 74° for Cu (2 2 0) [18,20,38–41]. Tungsten disulfide peaks are detected at about 14° for WS_2 (0 0 2), near to 29° for WS_2 (0 0 4), at 44° for WS_2 (0 0 6) and at about 59° for WS_2 (0 0 8) [11,18,20,42,43]. The intensity of the lubricant peaks coherently raises with the increase of its concentration (Fig. 4a) and, parallel, the opposite behavior is observed for Cu peaks (Fig. 4b). No evidence of the presence of undesired phases are found, irrespective of the employed WS_2 concentration. Specifically, Cu_2S characteristic peaks in the 20–35° range [44,45] are not detected, thus ruling out a reaction between copper and tungsten disulfide. Moreover, decomposition issues can also be ignored: tungsten typical peaks at 40° for W (1 1 0), at 57° for W (2 0 0), and at 72° for W (2 1 1) [46] are not observed. Therefore, the discussed preparation method can be considered sufficiently reliable in terms of chemical stability of the composites.

3.3 Raman scattering

All the spectra obtained by Raman scattering spectroscopy, reported in Fig. 5, exhibit four main contributions. The peaks around 295 and 350 cm^{-1} [47] and the peak at 520 cm^{-1} [48] refer to the two different oxidation states of copper, CuO and Cu_2O respectively. The presence of the second phase

WS_2 is represented by the mode at 420 cm^{-1} [49], while its peak at 350 cm^{-1} overlaps with that of CuO. The lack of unwanted phases, already assumed from XRD patterns, is confirmed by the absence of peaks around 265 and 474 cm^{-1}, attributed to CuS [50], and 472 cm^{-1}, related to Cu_2S [51].

3.4 Optical contact angle

Fig. 6 portrays average static contact angle measurements taken on the Cu-XWS_2 samples, along with the corresponding standard deviations extrapolated from ten measurements. The prepared composites reveal a hydrophobic behavior, with values ranging from 108.4±6.8° of Cu-25WS_2 to 131.0±1.8° of Cu-5WS_2. This last value slightly exceeds the one measured for benchmark Cu-10WS_2 (130.0±3.4° [26]). Except for Cu-25WS_2, the combination of the copper matrix with tungsten disulfide tends to accentuate the hydrophobicity of pure copper, previously investigated by our research group (OCA of 116.4±5.2° [26]). However, the addition of larger contents of tungsten disulfide reduces the static contact angle values, hence slightly enhancing the wettability of the composites, likely due to the hydrophilicity of virgin WS_2 powders [42]. Considering a potential application of copper-based composites in sliding electrical contacts working under harsh conditions, i.e., in the aerospace sector, a high hydrophobicity would be required to strongly limit the undesired formation of a uniform ice layer at high altitudes and low temperatures.

3.5 Scanning electron microscopy

SEM images of the cross-sections of Cu-10WS_2 and Cu-30WS_2 are collected in Fig. 7, to better appreciate the change in microstructure due to different WS_2 concentrations. The brighter phase has been identified as the solid lubricant, whereas the grey one is the copper matrix [25]. WS_2 particles appear homogeneously distributed within benchmark Cu-10WS_2 (Fig. 7(a1)-7(a3)) and mainly arranged in elongated clusters, whose presence visibly grows with the increase of the lubricating agent content up to 30 wt %. This homogeneity could be favorable from the standpoint of the composites frictional behavior, as reported in other works [52]. The black spots dispersed in the microstructure could be attributed to micro-porosity [18] resulting from a very localized interfacial debonding. It can be noticed that the spots are larger and more visible in Cu-30WS_2 (Fig. 7(b1)-7(b3)), for which a lower relative density is expected. The absence of darker zones associated to Cu_2S at the WS_2-Cu interface confirms a correct execution of the proposed preparation method, which permits to avoid undesired chemical reactions and, consequently, the preservation of the existing phases in the final composites as already deduced from X-ray diffraction outcomes (Section 3.2).

3.6 Density

Absolute and relative densities of the Cu-XWS_2 composites are summarized in Table 1, whereas relative density values are highlighted as a function of WS_2 content in Fig. 8. In general, the addition of WS_2 causes a slight decrease in density of the produced tablets, as expected considering the lower density of the second phase (7.50 g cm^{-3} [53]) with respect to pure copper (7.69±0.01 g cm^{-3}). Consequently, it can be hypothesized that low lubricant concentrations could contribute to optimize the compaction of the final product. Nevertheless, a residual internal porosity can be recognized for all the composites, as observed from SEM images; it could be likely related to the lower efficiency in filling voids of the cold-pressing and hot-sintering process with respect to those relying on hot-pressing, and probably to the short employed sintering time.

Table 1. Absolute and relative densities of reference Cu and of the Cu-XWS_2 composites.

Sample	Absolute density (g cm^{-3})	Relative density (%)
Cu	7.69 ± 0.01	85.83 ± 0.09
Cu-5WS_2	7.67 ± 0.01	85.62 ± 0.11
Cu-10WS_2	7.65 ± 0.01	85.36 ± 0.09
Cu-15WS_2	7.54 ± 0.02	84.19 ± 0.20
Cu-20WS_2	7.53 ± 0.01	83.99 ± 0.07
Cu-25WS_2	7.43 ± 0.01	82.94 ± 0.10
Cu-30WS_2	7.36 ± 0.01	82.17 ± 0.09

3.7 Electrical resistivity

Electrical resistivity measurements of the Cu-XWS_2 samples are reported in Fig. 9. The resistivity of the fabricated composites increases with raising lubricant content and composite porosity. This behavior is coherent considering the semiconducting nature of layered TMDs such as tungsten disulfide [54]. However, a too high resistivity is undesired in sliding electrical contacts, due to the necessity of ensuring an adequate current flow. Sensitivity to WS_2 content is contained up to 20 wt %, as the samples demonstrate acceptable resistivity values in the same order of magnitude of the employed copper powder [26], which is slightly less conductive than pure copper (1.68×10^{-8} Ω m [55]) due to porosity and oxidation issues [56]. On the contrary, a steep growth towards one order of magnitude higher-values is observed for Cu-25WS_2 and Cu-30WS_2. In these cases, the synergistic effect of second phase and increased micro-porosity, attested by density decrease, negatively influences the electrical properties of the composites up to unsatisfactory values.

3.8 Scratch test results

Fig. 10 depicts apparent friction coefficient and scratch hardness results of the Cu-XWS_2 samples. The lubricating ability of tungsten disulfide can be recognized by the slight reduction in friction coefficient exhibited by Cu-5WS_2 with respect to pure copper powder [26]. A slightly decreasing trend of FC with increasing lubricant concentration is apparent up to 20 wt % content, although for higher values of concentration data scatter becomes significantly larger, probably due to material inhomogeneity at the small scale probed by micro-scratch testing (Fig. 10(a)). This outcome suggests that no particular advantages in terms of FC are obtained by including high quantities of tungsten disulfide.

Scratch hardness performances of the Cu-XWS_2 composites are shown in Fig. 10(b). Composites up to 15 wt % WS_2 content are harder than pure copper. Conversely, larger concentrations of solid lubricant (20, 25, 30 wt %) result in a softer material, thanks to an evident decreasing trend of hardness with increasing content of WS_2.

Overall, scratch data would suggest that benchmark Cu-10WS_2 has the highest potential of succeeding when used for sliding electrical contacts working under harsh conditions: it combines a reduction of friction common to all composites with the highest hardness value.

Another desired feature offered by composites containing up to 10 wt % of WS_2 is shown by optical microscopy images of the scratch grooves, Fig. 11: there is no significant flake-like debris formation close to the groove borders, something which is very important in view of applications like slip rings. The results of the evaluated degree of penetration are reported in Fig. 12. The DoP values range from 0.275 to 0.350. Pure copper displays an average DoP value of 0.317, which can be associated to a micro-ploughing wear mechanism. The presence of low contents of solid lubricant (5 wt %, 10 wt %, and 15 wt %) decreases the DoP with respect to pure copper, suggesting a better resistance to micro-scratch. Conversely, higher concentrations of WS_2 (20 wt %, 25 wt %, and 30 wt %) lead to an increase of DoP up to 0.350 for Cu-30WS_2, due to a possible initial transition to a flaking-type wear. The change in scratch wear behavior could also be observed by the gradual thickening of the ridges while increasing the WS_2 content.

SEM images at different magnifications of the scratch groove on Cu-5WS_2 are shown in Fig. 13. It is possible to notice several agglomerates of solid lubricant as white spots spread out on the groove (Fig. 13(b)-13(c)); hence an effective lubricating action could not be presumed. Specific wear rates and wear coefficients, depicted in Fig. 14, have been calculated from the experimental data as explained in Section 2.11. The values trend is consistent with the computed scratch hardness: Cu-10WS_2, which has the highest hardness outcome (787.9±66.6 MPa), coherently exhibits the lowest specific wear rate ($1.14 \pm 0.08 \times 10^{-1}$ mm^3 N^{-1} m^{-1}) and wear coefficient ($8.96 \pm 0.64 \times 10^{-2}$). Therefore, it can be stated that a single pass test emphasizes the softening effect caused by higher solid lubricant concentrations on the composites, since the formation of a uniform tribo-film is not expected. Wear coefficient values corroborate this observation, as their order of magnitude (10^{-1}–10^{-2}) falls within the "wear by hard particles" regime [57] independently from the WS_2 content, even though friction coefficients are acceptable.

3.9 Vickers hardness

Vickers hardness values of the Cu-XWS_2 composites, reported in Fig. 15, appear to be consistent with scratch hardness ones, as expected [30,31]. The effect of tungsten disulfide on the Vickers hardness of copper-based composites differs from the one of other solid lubricants, such as carbonaceous phases. Previous studies have proved an overall hardness decrease provoked by the combination of a copper matrix with species of soft nature, such as graphite [24,25,58,59]. Conversely, WS_2 contributes to the strengthening of the manufactured samples with respect to virgin copper. As it can be noticed, a second phase concentration of 5 wt % leads to a Vickers hardness value of 67.5±1.2 HV. A further growth up to 71.0±1.5 HV is witnessed for benchmark Cu-10WS_2, then hardness performances tend to progressively decrease. This behavior is coherent with results obtained by other authors [18,60]. It could be explained by an active synergy between Cu and WS_2, promoted by the anisotropic lamellar structure of the TMD and its strong interfacial bonding with the metal matrix [19]. This beneficial effect is exerted up to a threshold amount of lubricant, which can be identified at about 10 wt %. Once this boundary is overcome, the probable redistribution of anisotropic WS_2 particles, visible in the particle size curves (Fig. 3) as a frequency peak at low diameter size (≈ 0.6 μm), hinders the beneficial impact on the mechanical properties of the composite, in particular on both scratch and indentation hardness.

3.10 Wear test results

Fig. 16 illustrates the friction coefficients of Cu-XWS_2 samples as a function of the sliding distance covered during wear tests (500 m). The wear curves have been automatically smoothed during the raw data processing. The lubricating effect of tungsten disulfide is evident (Fig. 16(a)), as friction coefficients values of the Cu-XWS_2 composites are significantly lower than 0.75, previously measured by our research group for a pure electrolytic copper tablet [26] and consistent with literature values [19]. The initial higher outcomes, exhibited by all the analyzed composites, could be attributed to a running stage in which the coupling between the counter ball and the Cu-XWS_2 disks is not completed. Once the actual mating is accomplished after a sliding distance that ranges from 150 m to 350 m depending on the sample, a reduction of friction coefficient is found and then a steady state condition is maintained, with values general ranging from 0.12 and 0.18 (Fig. 16(b)). As already discussed, the lubricating capability of WS_2 derives from its sandwich-like crystal structure. The dangling and unsaturated bonds on the edge of the WS_2 basal planes are prone to react with environmental moisture and oxygen to form tribo-oxidation products, such as WO_3. As a consequence, the developed lubricating layers can easily slide under shearing stress. The movement of the ball on the tablets surface is therefore facilitated [16,18].

Fig. 17 shows OM images of the wear tracks generated on the Cu-XWS_2 composites. At first sight, the increasing content of second phase can be appreciated through the color change of the contact area from a typical copper shade (Cu-5WS_2) to a light blue-gray one (Cu-30WS_2). A non-homogeneous appearance of all wear scars can be witnessed, similarly to benchmark Cu-10WS_2 [26]. It could be attributed to a chipping phenomenon caused by the sliding of the counter ball. Therefore, an abrasive wear mechanism can be hypothesized at low WS_2 content, while at high WS_2 concentration the lubricant particles exposed on the surface within the tribo-film may more easily stick to the counter surface, leading to an additional adhesive mechanism. This effect possibly explains the pits visible in the samples with 25 and 30 wt % of WS_2. The track width of Cu-5WS_2 (1309 μm) is comparable to benchmark Cu-10WS_2 (1255 μm) due to the higher hardness of these samples, which provokes a broadening of the counter ball contact zone. Cu-20WS_2 and Cu-30WS_2 display wear tracks with variable width (716–1032 μm and 726–876 μm, respectively). A possible explanation is the formation of surface asperities that act as third bodies, progressively hindering the correct contact between the surfaces and outrunning them. The effective action of the solid lubricant can be observed at higher content, with Cu-25WS_2 exhibiting the smoother wear track with almost constant width (843 μm). The homogeneity of the contact area could be associated to the ability of WS_2 in promoting an adhesive wear mechanism, preventing a direct metal-to-metal interaction via the formation of a lubricating film that becomes more continuous at increased WS_2 concentration [19].

SEM morphologies of post-wear test samples are gathered in Fig. 18. Specifically, Cu-5WS_2, Cu-15WS_2, and Cu-30WS_2 have been chosen as lower limit, middle value, and upper limit of second phase concentration to facilitate the comprehension of how WS_2 impacts on the wear behavior of the composites. The uneven aspect of Cu-5WS_2 wear track (Fig. 18(a1)) is confirmed by SEM analysis. Micro-cracks and pile-up of removed material are the consequence of an initial abrasive mechanism, due to which the sample is plastically deformed, and flaky particles are formed. The progressive increase of second phase content guarantees a transition towards the formation of a more uniform tribo-layer, by which WS_2 exerts its lubricating effect, limiting the contact between the composites and the counterpart [18,25]. An adhesive mechanism may be therefore triggered and WS_2 fosters the detachment of small portions of the tribo-film. Nevertheless, the adhesive contribution on the overall wear mechanism does not overcome the abrasive contribution even at high WS_2 concentration. SEM image at 400x of Cu-30WS_2 (Fig. 18(c1)) is obtained in a narrowing zone, hence track borders are visible. As previously asserted, this periodic width variation may be related to the presence of third bodies that complicate the sliding of the counter ball and cause the generation of rough-edged debris (Fig. 18(c2)). Cross-sectional images perpendicular to the sliding direction allow to observe the profile of stratified material due to detachment and reattachment forced by the counter ball movement. Fig. 19 shows specific wear rates and wear coefficients of the Cu-XWS_2 composites, computed as described in Section 2.11 by exploiting the profiles as exemplified in Fig. 2. The results demonstrate a decrease in wear coefficient (Fig. 19(b)) as the second phase content increases. The best performance is exhibited by the samples with the highest WS_2 concentration (Cu-25WS_2 and Cu-30WS_2), but it can be underlined that Cu-15WS_2 has a wear coefficient within the same order of magnitude (10^{-5}) of the above-mentioned composites despite a lower second phase content. The calculated wear coefficients fall within the "mild" wear regime, which is typically characterized by the formation of fine debris [57] as confirmed by OM and SEM analyses. The discrepancy between these values and the ones extrapolated from scratch tests (order of magnitude of 10^{-1}–10^{-2}) can be mainly attributed to the experimental setup differences: the multiple-pass of the counter ball on the tested surface leads to the activation of the lubricating effect of WS_2 and, consequently, further confirms the formation of a tribo-film. The positive aspect of the discussed outputs is that a wear test better approximates the actual operating conditions of a sliding electrical contact, therefore the performance of the prepared composites can be considered adequate.

4. Conclusions

- The present study reports an investigation about the effects of second phase content between 5 and 30 wt % on the tribological, mechanical, electrical and wettability properties of self-lubricating Cu-WS_2 composites for a potential application in sliding electrical contacts working under harsh conditions. The samples have been manufactured via a powder metallurgy process, consisting of a ball milling step, a cold-pressing and a pressureless hot-sintering process.
- The experimental outcomes pointed out that WS_2 substantially improves the wettability and the wear behavior of the investigated composites with respect to pristine copper.
- Scratch and Vickers hardness of the samples are enhanced up to a 15 wt % content of second phase, while electrical conductivity is not excessively hindered. However, a filler amount larger than 20 wt % led to material softening, a one order of magnitude increase in resistivity and also a slight reduction in hydrophobicity. Considering that adequate electrical conductivity and high hydrophobicity are paramount for an application in sliding electrical contacts, the inclusion of larger contents of WS_2 in these composites is not recommended, at least for the particular application considered.
- From the interpretation of wear test results, an abrasive wear mechanism can be hypothesized for low WS_2 contents, whereas the solid lubricant shall promote a transition towards an adhesive mechanism at high concentrations, thus ensuring a better self-lubricating behavior

of the composites. Extrapolated specific wear rates and wear coefficients support this statement, since lower values are obtained once the WS_2 content exceeds 10 wt %.

- It can be concluded that the optimal trade-off between tribological, electrical and wettability properties should be surveyed in the range of 10–15 wt % of tungsten disulfide. Further analyses are mandatory to gain a better understanding of the actual degradation mechanism of Cu-WS_2 composites.

Acknowledgements

The authors would like to thank the EIT Raw Materials that funded this work within the project ADMA 2 – Practical training between Academia and Industry during doctoral studies (Project n. 18252), Logic S.p.A. for the supply of materials and instruments, and Eng. Alessia Arrigoni of the Organic Functional and Nanostructured Materials (FuNMat) laboratory, Department of Chemistry, Materials and Chemical Engineering "Giulio Natta", Politecnico di Milano, for the useful help in the acquisition and interpretation of Raman scattering spectra.

References

[1] Shin WG, Lee SH. An analysis of the main factors on the wear of brushes for automotive small brush-type DC motor. J Mech Sci Technol 2010;24:37–41. https://doi.org/10.1007/s12206-009-1135-4.

[2] Holm R. Electric Contacts. Berlin, Heidelberg: Springer Berlin Heidelberg; 1967. https://doi.org/10.1007/978-3-662-06688-1.

[3] Xiao JK, Liu LM, Zhang C, Zhang L, Zhou KC. Sliding electrical contact behavior of brass fiber brush against coin-silver and Au plating. Wear 2016;368–369:461–9. https://doi.org/10.1016/j.wear.2016.10.007.

[4] Slade PG. Electrical Contacts, Principles and Applications. Second Edi. Boca Raton, FL: CRC Press - Taylor & Francis Group; 2014.

[5] Wang QJ, Chung Y-W, editors. Encyclopedia of Tribology. Boston, MA: Springer US; 2013. https://doi.org/10.1007/978-0-387-92897-5.

[6] Argibay N, Sawyer WG. Low wear metal sliding electrical contacts at high current density. Wear 2012;274–275:229–37. https://doi.org/10.1016/j.wear.2011.09.003.

[7] Bares JA, Argibay N, Dickrell PL, Bourne GR, Burris DL, Ziegert JC, et al. In situ graphite lubrication of metallic sliding electrical contacts. Wear 2009;267:1462–9. https://doi.org/10.1016/j.wear.2009.03.024.

[8] Furlan KP, de Mello JDB, Klein AN. Self-lubricating composites containing MoS2: A review. Tribol Int 2018;120:280–98. https://doi.org/10.1016/J.TRIBOINT.2017.12.033.

[9] Tyagi R, Das AK, Mandal A. Electrical discharge coating using WS2 and Cu powder mixture for solid lubrication and enhanced tribological performance. Tribol Int 2018;120:80–92. https://doi.org/10.1016/J.TRIBOINT.2017.12.023.

[10] Zhu S, Cheng J, Qiao Z, Yang J. High temperature solid-lubricating materials: A review. Tribol Int 2019;133:206–23. https://doi.org/10.1016/J.TRIBOINT.2018.12.037.

[11] Kang X, Zhang L. Enhanced sliding electrical contact properties of silver matrix self-lubricating nanocomposite using molecular level mixing process and spark plasma sintering. Powder Technol 2020;372:94–106. https://doi.org/10.1016/j.powtec.2020.05.062.

[12] Xiao J, Wu Y, Zhang W, Chen J, Zhang C. Friction of metal-matrix self-lubricating composites: Relationships among lubricant content, lubricating film coverage, and friction coefficient. Friction 2020;8:517–30. https://doi.org/10.1007/s40544-019-0270-x.

[13] Yuan J, Yao Y, Zhuang M, Du Y, Wang L, Yu Z. Effects of Cu and WS2 addition on microstructural evolution and tribological properties of self-lubricating anti-wear coatings prepared by laser cladding. Tribol Int 2021;157:106872. https://doi.org/10.1016/J.TRIBOINT.2021.106872.

[14] Grandin M, Wiklund U. Wear phenomena and tribofilm formation of copper/copper-graphite sliding electrical contact materials. Wear 2018;398–399:227–35.

https://doi.org/10.1016/j.wear.2017.12.012.

[15] Natarajan N, Krishnaraj V, Davim JP. Metal Matrix Composites - Synthesis, Wear Characteristics, Machinability Study of MMC Brake Drum. 2015.

[16] Prasad S., McDevitt N., Zabinski J. Tribology of tungsten disulfide films in humid environments: Wear 1999;230:24–34. https://doi.org/10.1016/s0043-1648(99)00082-4.

[17] Wong KC, Lu X, Cotter J, Eadie DT, Wong PC, Mitchell KAR. Surface and friction characterization of MoS2 and WS2 third body thin films under simulated wheel/rail rolling-sliding contact. Wear 2008;264:526–34. https://doi.org/10.1016/j.wear.2007.04.004.

[18] Zhao L, Yao P, Gong T, Zhou H, Deng M, Wang Z, et al. Effect of Adding Tungsten Disulfide to a Copper Matrix on the Formation of Tribo-Film and on the Tribological Behavior of Copper/Tungsten Disulfide Composites. Tribol Lett 2019;67:1–13. https://doi.org/10.1007/s11249-019-1200-9.

[19] Xiao JK, Zhang W, Zhang C. Microstructure evolution and tribological performance of Cu-WS2 self-lubricating composites. Wear 2018;412–413:109–19. https://doi.org/10.1016/j.wear.2018.07.024.

[20] Zhou J, Ma C, Kang X, Zhang L, Liu X. Effect of WS2 particle size on mechanical properties and tribological behaviors of Cu-WS2 composites sintered by SPS. Trans Nonferrous Met Soc China 2018;28:1176–85. https://doi.org/10.1016/S1003-6326(18)64755-7.

[21] Srivastava SK, Avasthi BN. Layer type tungsten dichalcogenide compounds: their preparation, structure, properties and uses. J Mater Sci 1985;20:3801–15. https://doi.org/10.1007/BF00552369.

[22] Nian J, Chen L, Guo Z, Liu W. Computational investigation of the lubrication behaviors of dioxides and disulfides of molybdenum and tungsten in vacuum. Friction 2017;5:23–31. https://doi.org/10.1007/s40544-016-0128-4.

[23] Brainard JA. The thermal stability and friction of the disulfides, diselenides, and ditellurides of molybdenum and tungsten in vaccum (10 -9 to 10 -6 TORR). 1969.

[24] Xiao JK, Zhang L, Zhou KC, Wang XP. Microscratch behavior of copper-graphite composites. Tribol Int 2013;57:38–45. https://doi.org/10.1016/j.triboint.2012.07.004.

[25] Wang Q, Chen M, Shan Z, Sui C, Zhang L, Zhu S, et al. Comparative study of mechanical and wear behavior of Cu/WS 2 composites fabricated by spark plasma sintering and hot pressing. J Mater Sci Technol 2017;33:1416–23. https://doi.org/10.1016/j.jmst.2017.06.014.

[26] Freschi M, Di Virgilio M, Zanardi G, Mariani M, Lecis N, Dotelli G. Employment of micro- and Nano-WS2 structures to enhance the tribological properties of copper matrix composites. Lubricants 2021;9. https://doi.org/10.3390/lubricants9050053.

[27] Lide DR, Data SR, Board EA, Baysinger G, Chemistry S, Library CE, et al. Section 4 - Properties of the Elements and Inorganic Compounds. CRC Handb. Chem. Phys., CRC Press; 2020, p. 722–875. https://doi.org/10.1201/b17118-9.

[28] Bowden FP, Tabor D. The Friction and Lubrication of Solids. Oxford: Clarendon Press, 1964; 1964.

[29] Briscoe BJ, Evans PD, Biswas SK, Sinha SK. The hardnesses of poly(methylmethacrylate). Tribol Int 1996;29:93–104. https://doi.org/10.1016/0301-679X(95)00045-6.

[30] Kurkcu P, Andena L, Pavan A. An experimental investigation of the scratch behaviour of polymers: 1. Influence of rate-dependent bulk mechanical properties. Wear 2012;290–291:86–93. https://doi.org/10.1016/j.wear.2012.05.005.

[31] Kurkcu P, Andena L, Pavan A. An experimental investigation of the scratch behaviour of polymers: 2. Influence of hard or soft fillers. Wear 2014;317:277–90. https://doi.org/10.1016/j.wear.2014.03.011.

[32] Kayaba T, Hokkirigawa K, Kato K. Analysis of the abrasive wear mechanism by successive observations of wear processes in a scanning electron microscope. Wear 1986;110:419–30. https://doi.org/10.1016/0043-1648(86)90115-8.

[33] Zum Gahr KH. Chapter 5 Grooving Wear. Tribol. Ser., vol. 10, 1987, p. 132–350. https://doi.org/10.1016/S0167-8922(08)70723-5.

[34] Archard JF. Contact and Rubbing of Flat Surfaces. J Appl Phys 1953;24:981–8. https://doi.org/10.1063/1.1721448.

[35] Archard JF, Hirst W. The wear of metals under unlubricated conditions. Proc R Soc London Ser A Math Phys Sci 1956;236:397–410. https://doi.org/10.1098/rspa.1956.0144.

[36] Huang J, Zhang Y, Wang D, Ren B, Song P, Zhang G, et al. Effect of ball milling process on the mechanical and thermal properties of the nanodiamond/2024Al composites. Micron 2021;148:103104. https://doi.org/10.1016/j.micron.2021.103104.

[37] Balasubramanian P, Battabyal M, Chandra Bose A, Gopalan R. Effect of ball-milling on the phase formation and enhanced thermoelectric properties in zinc antimonides. Mater Sci Eng B Solid-State Mater Adv Technol 2021;271:115274. https://doi.org/10.1016/j.mseb.2021.115274.

[38] Theivasanthi T, Alagar M. X-Ray Diffraction Studies of Copper Nanopowder. Sch Res Libr 2010;2:373–83.

[39] Cartigueyen S, Mahadevan K. Wear characteristics of copper-based surface-level microcomposites and nanocomposites prepared by friction stir processing. Friction 2016;4:39–49. https://doi.org/10.1007/s40544-016-0102-1.

[40] Cheng J, Mao M, Gan X, Lei Q, Li Z, Zhou K. Microstructures, mechanical properties, and grease-lubricated sliding wear behavior of Cu-15Ni-8Sn-0.8Nb alloy with high strength and toughness. Friction 2021;9:1061–76. https://doi.org/10.1007/s40544-020-0399-7.

[41] Khan A, Rashid A, Younas R, Chong R. A chemical reduction approach to the synthesis of copper nanoparticles. Int Nano Lett 2016;6:21–6. https://doi.org/10.1007/s40089-015-0163-6.

[42] Rodrigues SP, Polcar T, Carvalho S, Cavaleiro A. The wettability and tribological behaviour of thin F-doped WS2 films deposited by magnetron sputtering. Surf Coatings Technol 2019;378:125033. https://doi.org/10.1016/j.surfcoat.2019.125033.

[43] Kang X, Yu S, Yang H, Sun Y, Zhang L. Tribological behavior and microstructural evolution of lubricating film of silver matrix self-lubricating nanocomposite. Friction 2021;9:941–51.

https://doi.org/10.1007/s40544-020-0379-y.

[44] Pathan HM, Desai JD, Lokhande CD. Modified chemical deposition and physico-chemical properties of copper sulphide (Cu 2 S) thin films. Appl Surf Sci 2002;202:47–56. https://doi.org/10.1016/S0169-4332(02)00843-7.

[45] Saadeldin M, Soliman HS, Ali HAM, Sawaby K. Optical and electrical characterizations of nanoparticle Cu2S thin films. Chinese Phys B 2014;23. https://doi.org/10.1088/1674-1056/23/4/046803.

[46] Xiong L, He T. Synthesis and characterization of ultrafine tungsten and tungsten oxide nanoparticles by a reverse microemulsion-mediated method. Chem Mater 2006;18:2211–8. https://doi.org/10.1021/cm052320t.

[47] Tran TH, Nguyen VT. Phase transition of Cu2O to CuO nanocrystals by selective laser heating. Mater Sci Semicond Process 2016;46:6–9. https://doi.org/10.1016/j.mssp.2016.01.021.

[48] Lu C, Li Z, Ren L, Su N, Lu D, Liu Z. In Situ Oxidation of Cu2O Crystal for Electrochemical Detection of Glucose. Sensors 2019;19:2926. https://doi.org/10.3390/s19132926.

[49] Berkdemir A, Gutiérrez HR, Botello-Méndez AR, Perea-López N, Elías AL, Chia C-I, et al. Identification of individual and few layers of WS2 using Raman Spectroscopy. Sci Rep 2013;3:1755. https://doi.org/10.1038/srep01755.

[50] Chaki SH, Tailor JP, Deshpande MP. Covellite CuS – Single crystal growth by chemical vapour transport (CVT) technique and characterization. Mater Sci Semicond Process 2014;27:577–85. https://doi.org/10.1016/j.mssp.2014.07.038.

[51] Fu S-Y, Chang H-H, Hsu Y-K, Lin Y-G. Facile synthesis of Cu2S nanoarchitectures in application of surface enhanced Raman scattering. Proc. SPIE 9161, Nanophotonic Mater. XI, vol. 9161, SPIE; 2014, p. 916108. https://doi.org/10.1117/12.2059523.

[52] Rajkumar K, Aravindan S. Tribological studies on microwave sintered copper-carbon nanotube composites. Wear 2011;270:613–21. https://doi.org/10.1016/j.wear.2011.01.017.

[53] Sigma-Aldrich. Tungsten Disulfide Safesheet 2020:1–8.

[54] Sik Hwang W, Remskar M, Yan R, Protasenko V, Tahy K, Doo Chae S, et al. Transistors with chemically synthesized layered semiconductor WS 2 exhibiting 10 5 room temperature modulation and ambipolar behavior. Appl Phys Lett 2012;101. https://doi.org/10.1063/1.4732522.

[55] Lide DR, Data SR, Board EA, Baysinger G, Chemistry S, Library CE, et al. Section 12 - Properties of Solids. CRC Handb. Chem. Phys., CRC Press; 2020, p. 2085–322. https://doi.org/10.1201/b17118-17.

[56] Gelbstein Y, Haim Y, Kalabukhov S, Kasiyan V, Hartmann S, Rothe S, et al. Correlation between Thermal and Electrical Properties of Spark Plasma Sintered (SPS) Porous Copper. Sinter. Tech. Mater., InTech; 2015. https://doi.org/10.5772/59010.

[57] Springer handbook of materials measurement methods. Mater Today 2006;9:52. https://doi.org/10.1016/S1369-7021(06)71582-6.

[58] Futami T, Ohira M, Muto H, Sakai M. Indentation contact behavior of copper–graphite particulate composites: Correlation between the contact parameters and the electrical resistivity. Carbon N Y 2008;46:671–8. https://doi.org/10.1016/j.carbon.2008.01.023.

[59] Futami T, Ohira M, Muto H, Sakai M. Contact/scratch-induced surface deformation and damage of copper-graphite particulate composites. Carbon N Y 2009;47:2742–51. https://doi.org/10.1016/j.carbon.2009.05.034.

[60] Rajakumar N, Subramanian K, Sozhan G, Ramasamy K. Tribological studies of the sintered bronze—tungsten disulfide composites. Mater Res Express 2019;6:086568. https://doi.org/10.1088/2053-1591/ab1a8c.

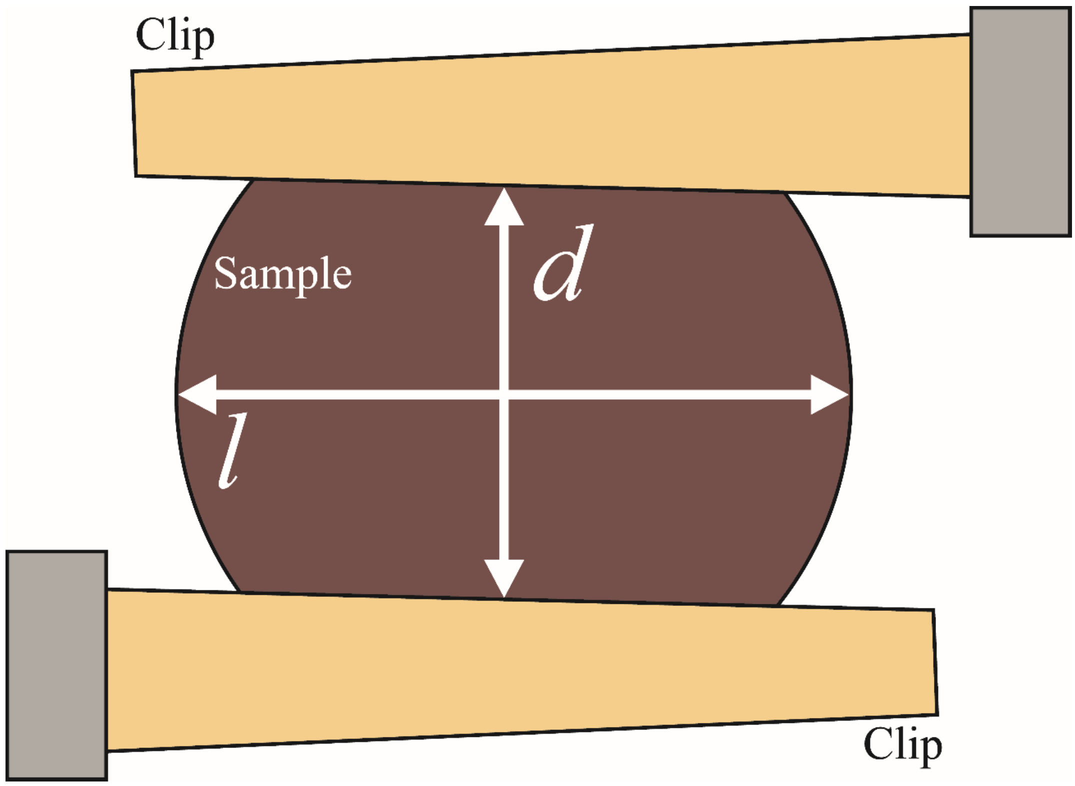

Fig. 1 Sketch of the geometrical parameters used to determine the electrical resistivity of the Cu-XWS_2 composites.

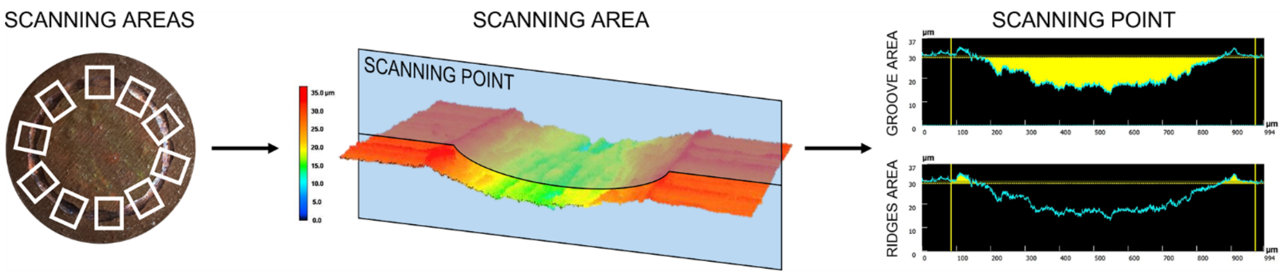

Fig. 2 Example of wear track profile analysis to evaluate the groove and the displaced material cross-sections.

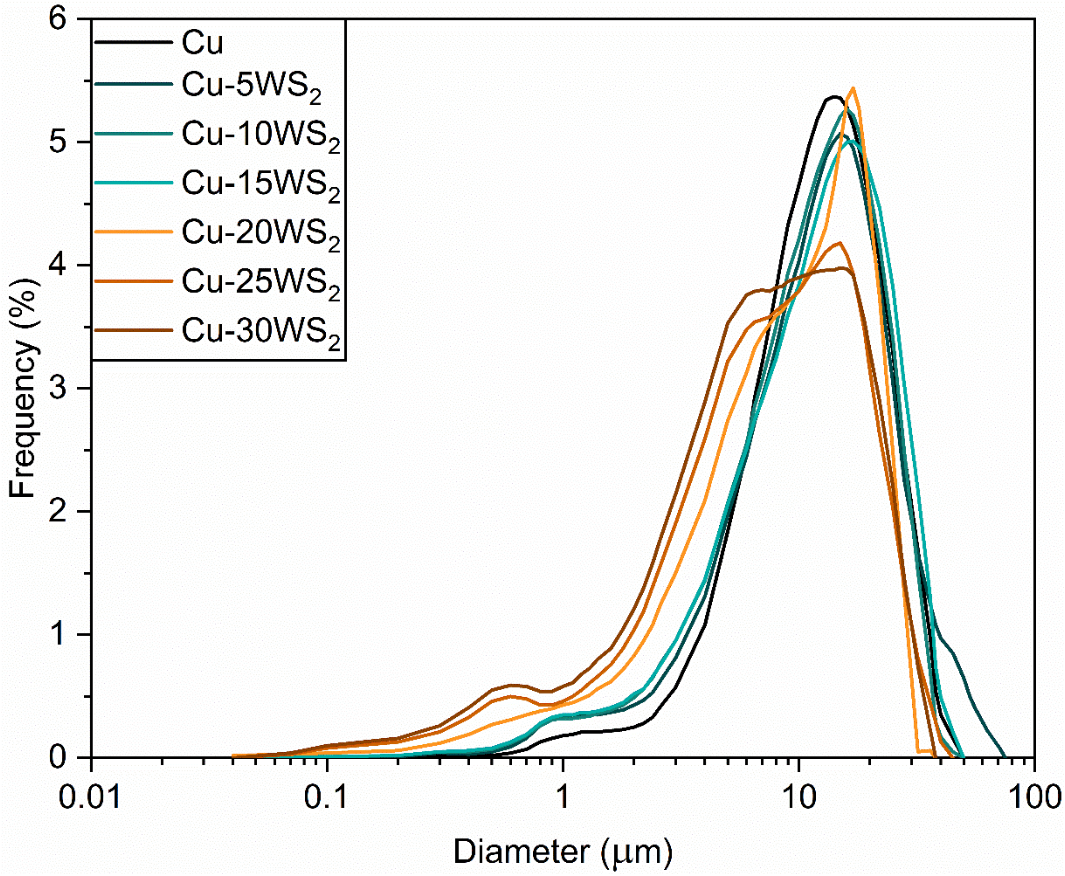

Fig. 3 Particle size distributions of reference Cu and of the Cu-XWS_2 composites.

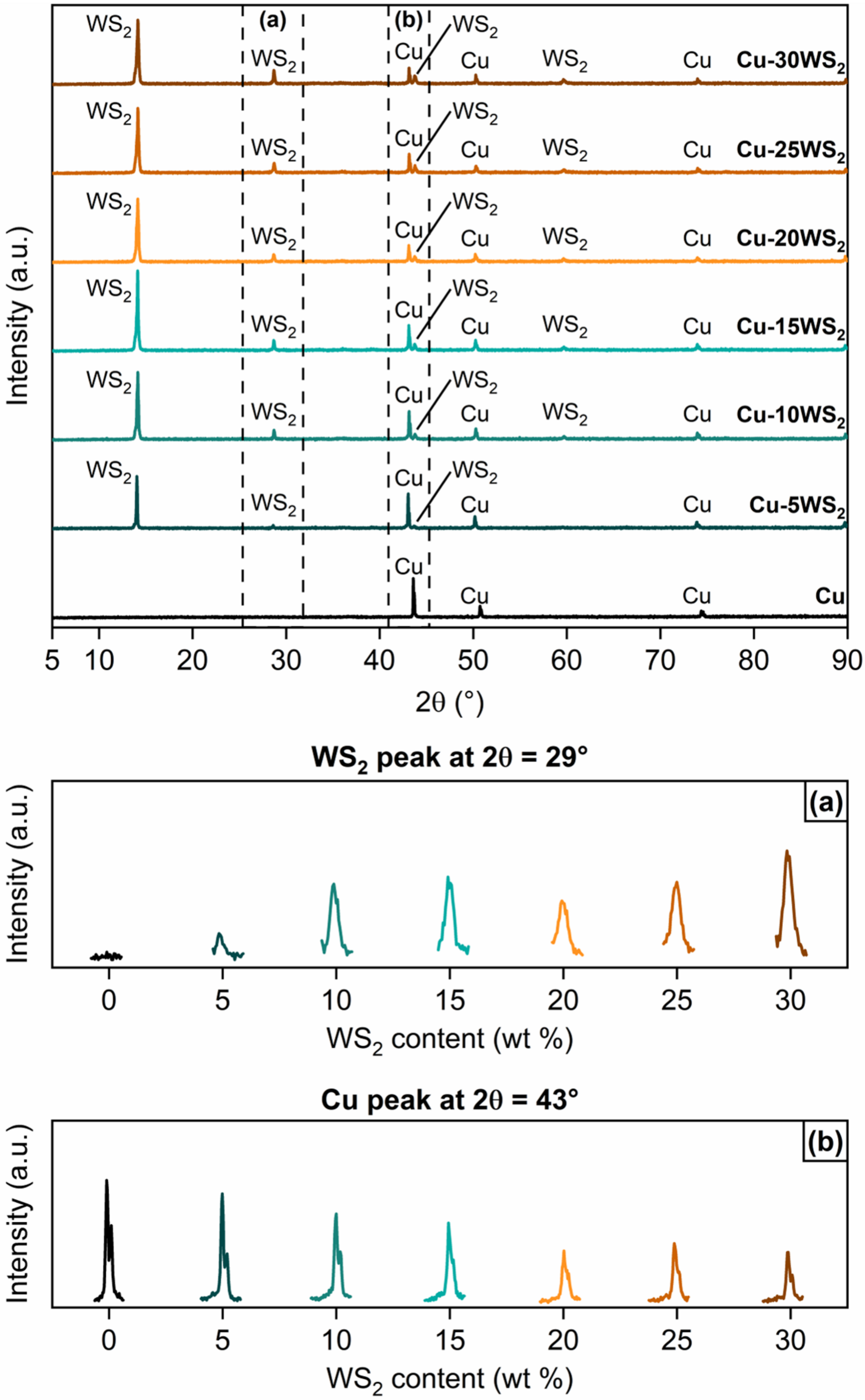

Fig. 4 XRD patterns of reference Cu and of the Cu-XWS_2 composites; (a) intensity trend of the WS_2 peak at 29° depending on WS_2 content; (b) intensity trend of the Cu peak at 43° depending on WS_2 content.

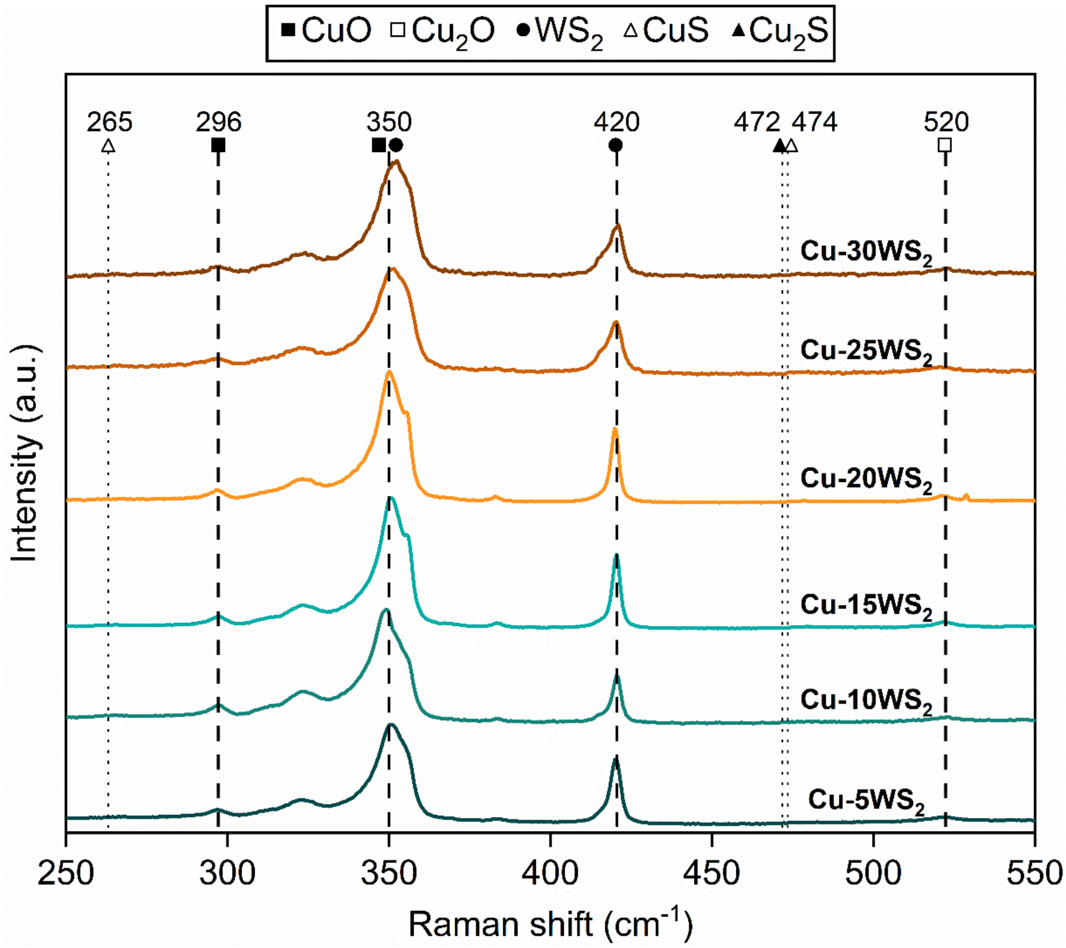

Fig. 5 Raman scattering spectra of Cu-XWS$_2$ composites.

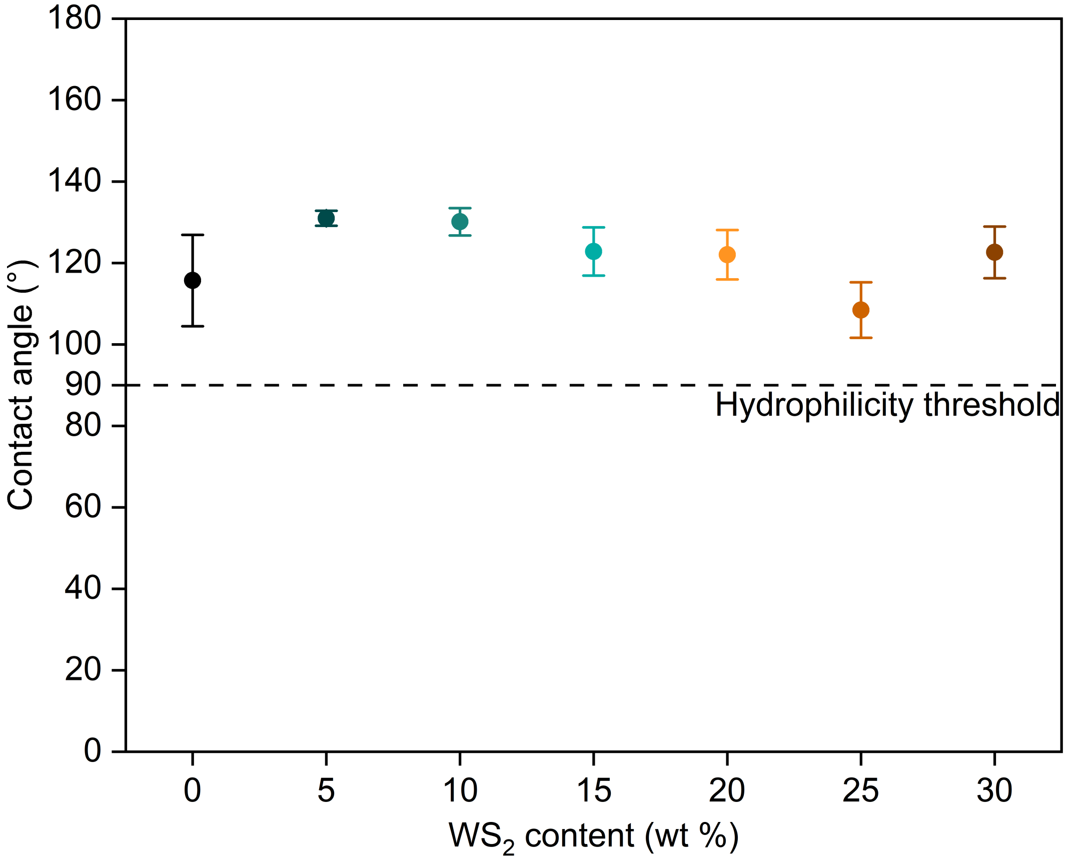

Fig. 6 Optical contact angle results of reference Cu and of the Cu-XWS_2 composites.

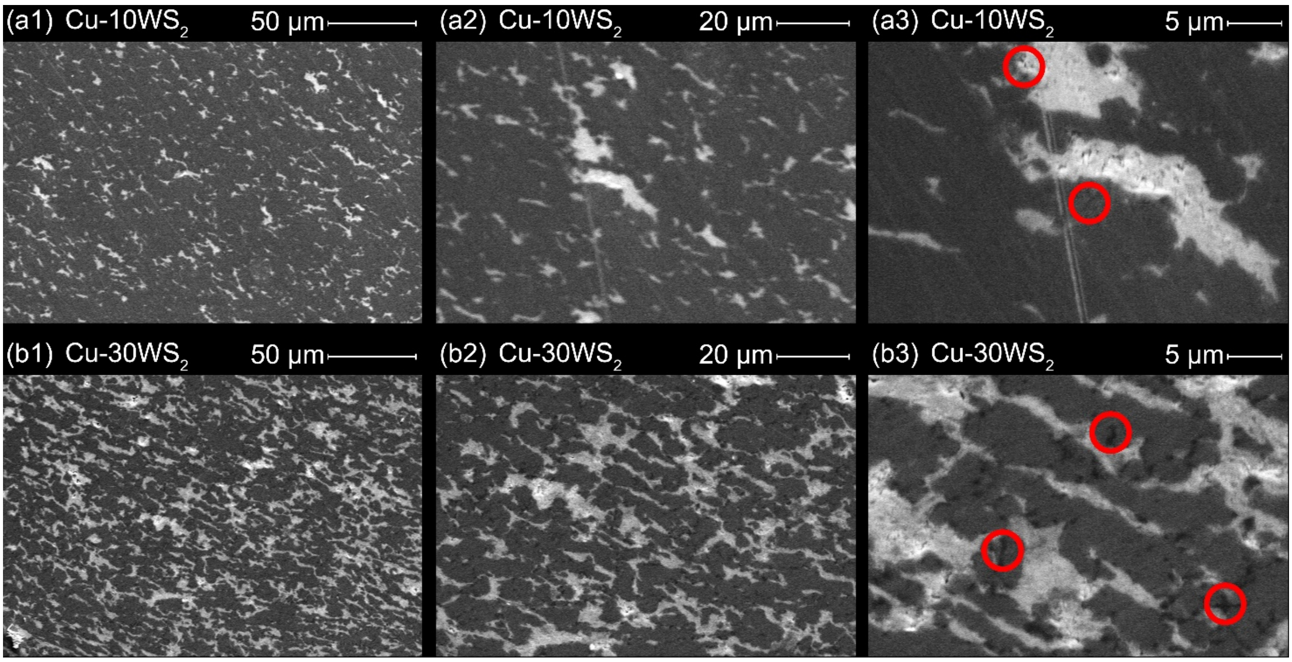

Fig. 7 SEM images of the cross-section of Cu-XWS_2 composites: Cu-10WS_2 at 500x (a1), 1000x (a2), and 3000x (a3), Cu-30WS_2 at 500x (b1), 1000x (b2), and 3000x (b3).

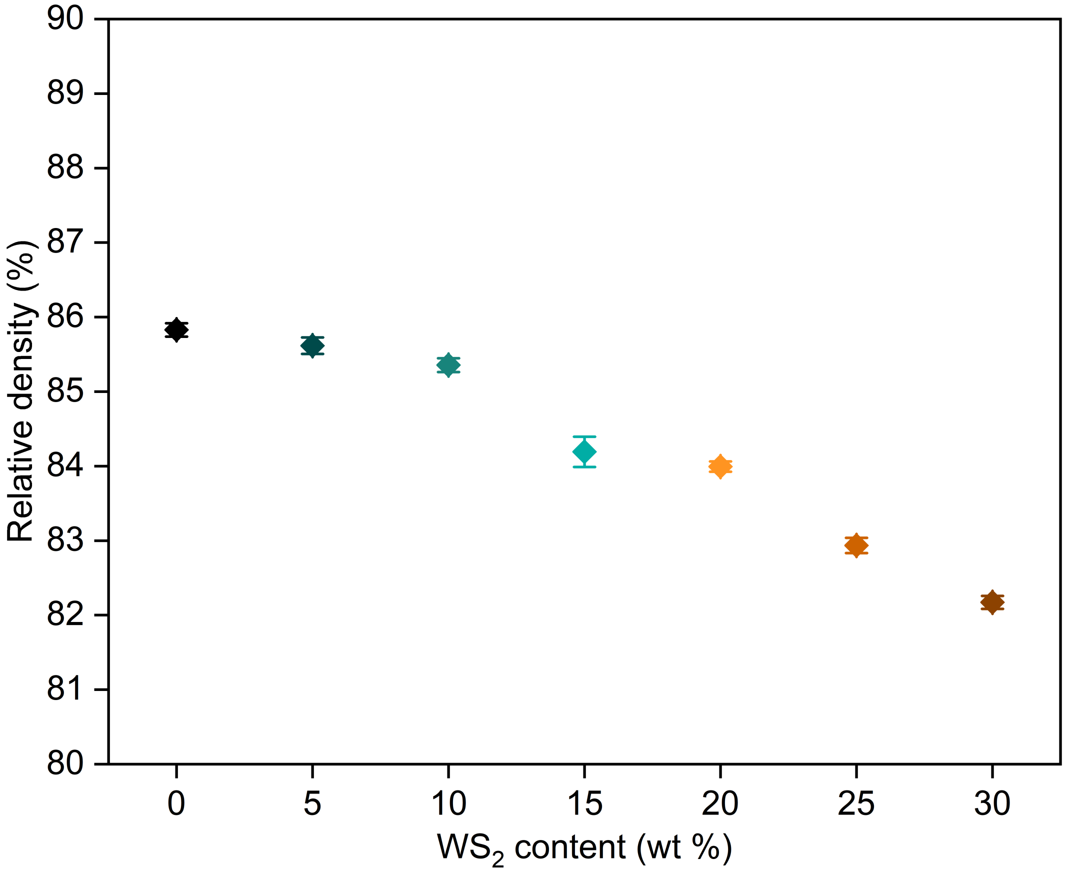

Fig. 8 Relative density values of reference Cu and of the Cu-XWS_2 composites.

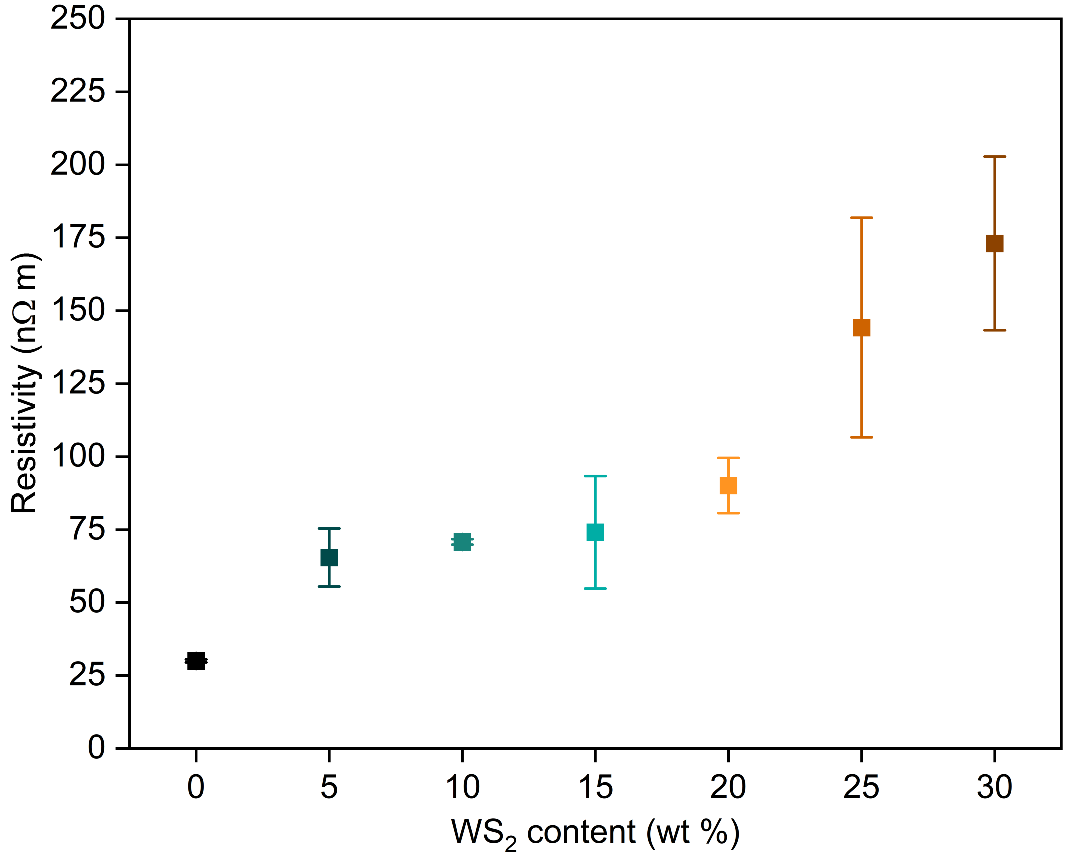

Fig. 9 Electrical resistivity values of reference Cu and of the Cu-XWS_2 composites.

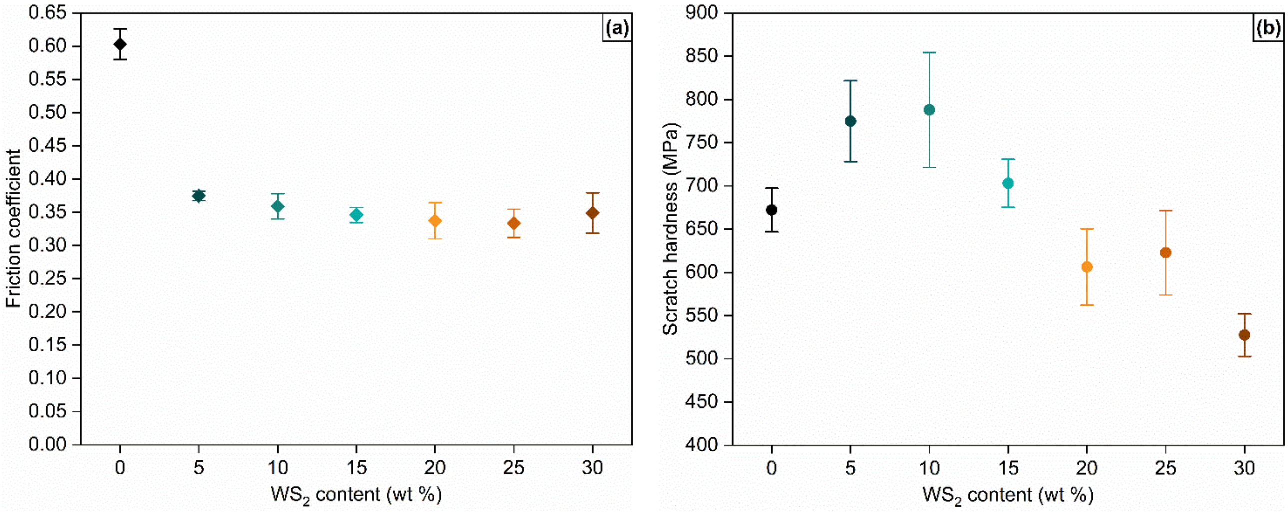

Fig. 10 (a) Friction coefficients and (b) scratch hardness values of reference Cu and of the Cu-XWS_2 composites.

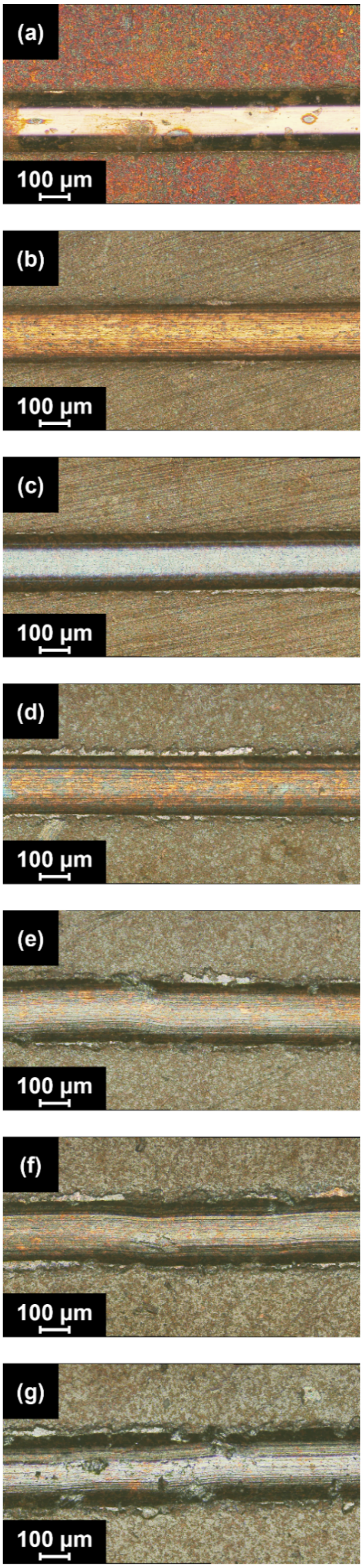

Fig. 11 OM images of the scratches of (a) reference Cu and of the Cu-XWS_2 composites at 20x magnification: (b) Cu-5WS_2, (c) Cu-10WS_2, (d) Cu-15WS_2, (e) Cu-20WS_2, (f) Cu-25WS_2, (g) Cu-30WS_2.

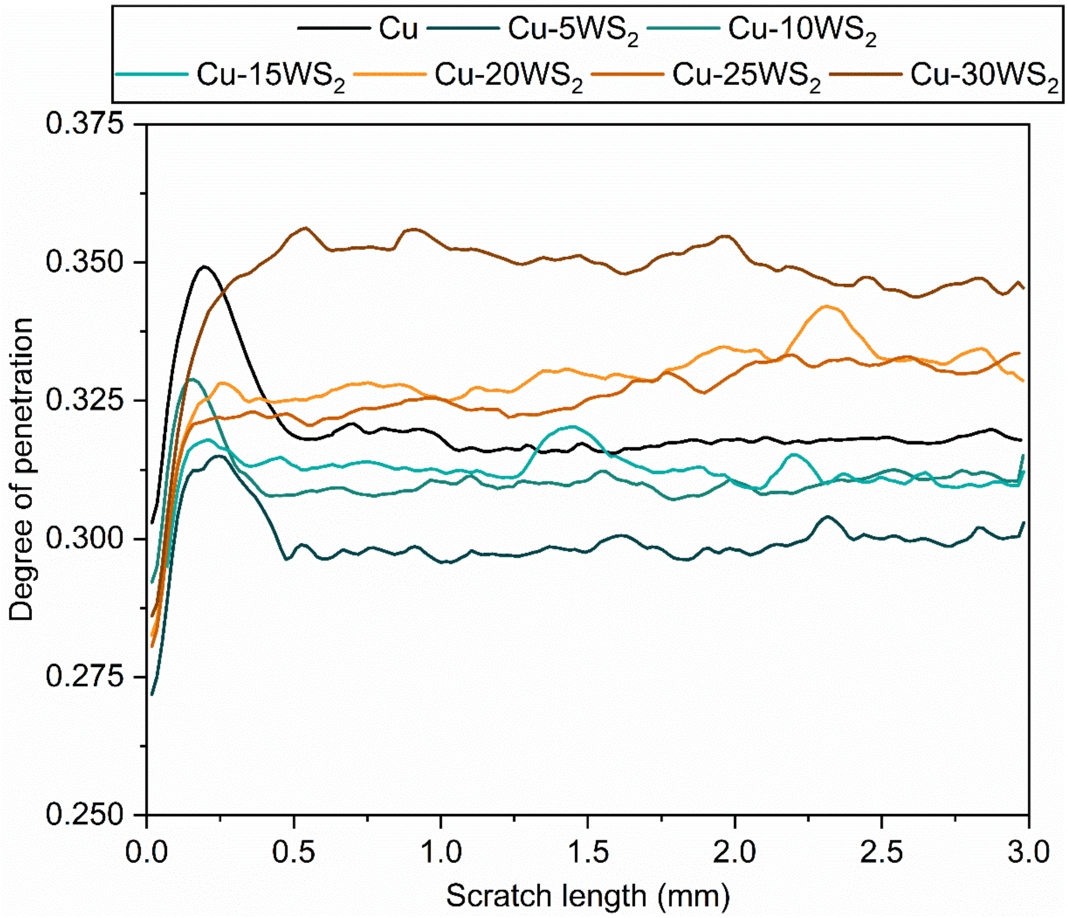

Fig. 12 Degree of penetration values from the scratch tests performed on reference Cu and on the Cu-XWS_2 composites.

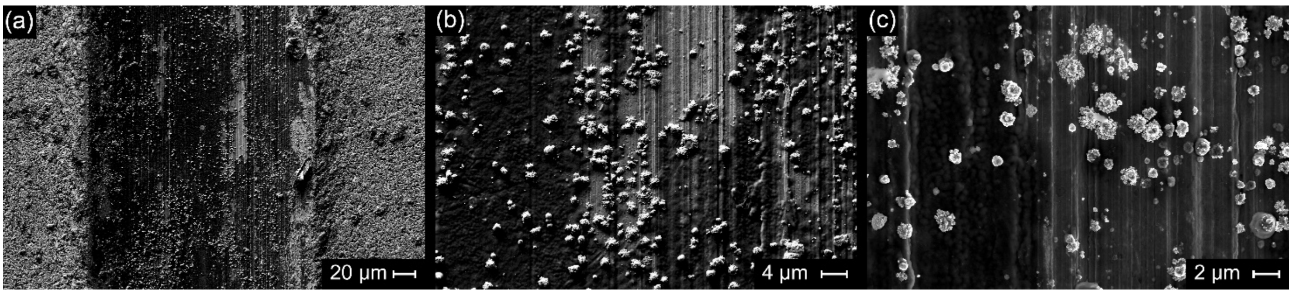

Fig. 13 SEM images of the scratches of Cu-5WS_2 at different magnifications: (a) 800x, (b) 5000x, (c) 10000x.

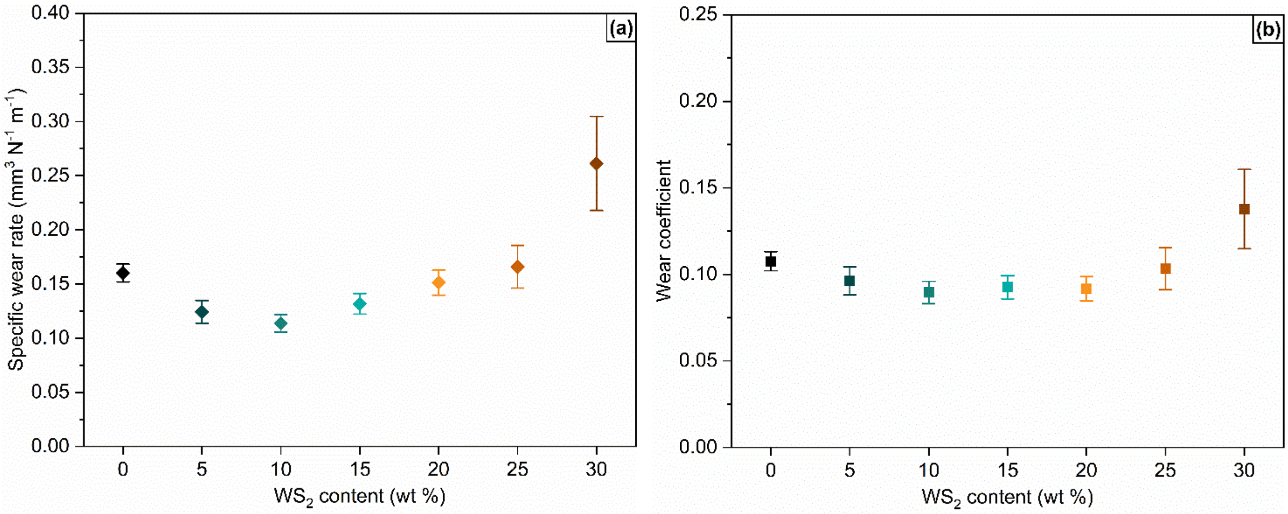

Fig. 14 (a) Specific wear rates and (b) wear coefficients of reference Cu and of the Cu-XWS_2 composites extrapolated from scratch tests.

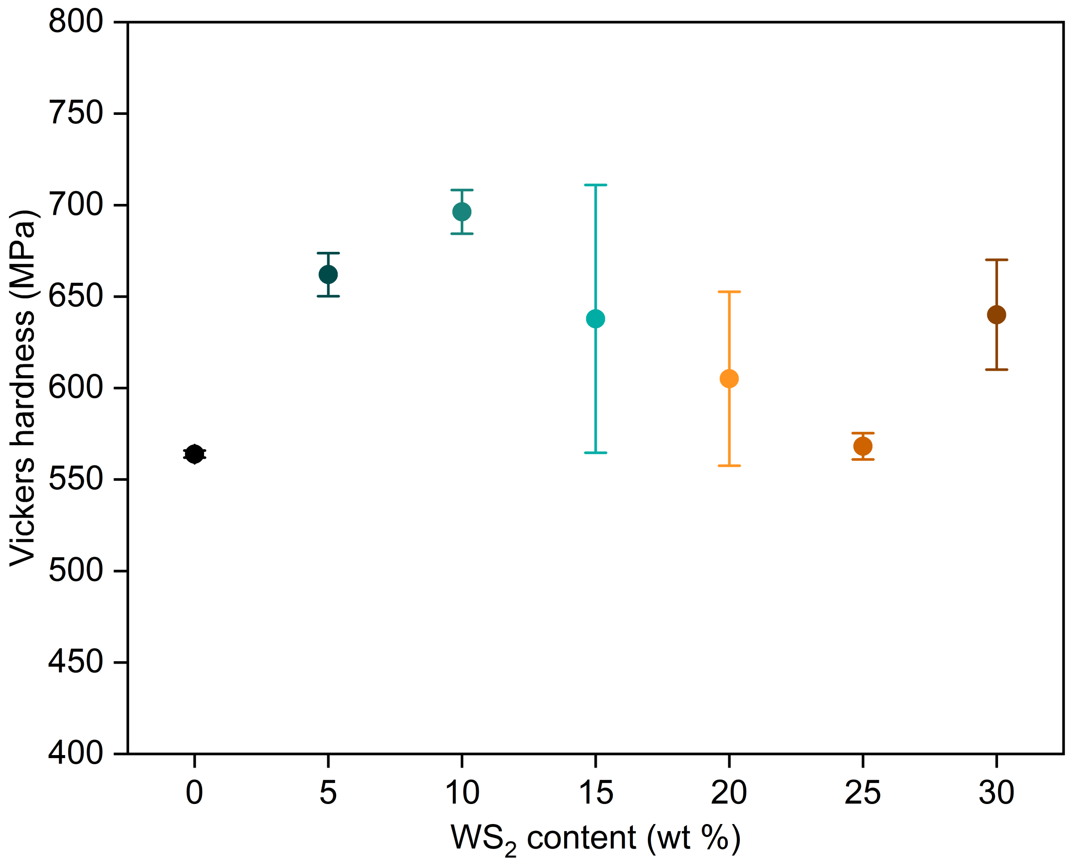

Fig. 15 Vickers hardness values of reference Cu and of the Cu-XWS_2 composites.

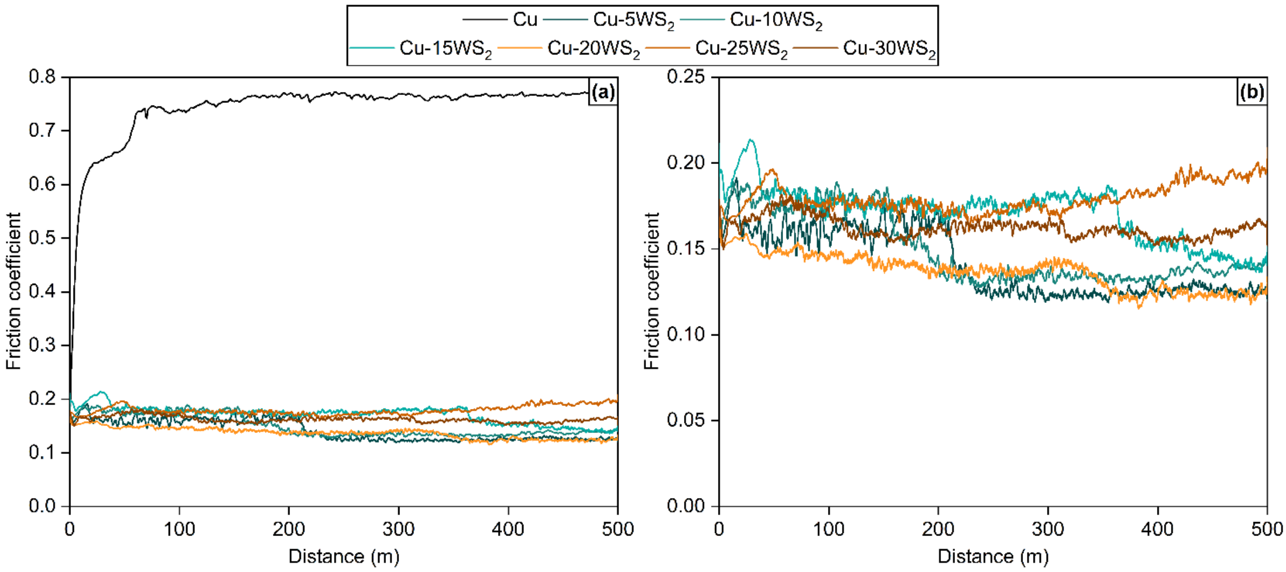

Fig. 16 (a) Friction coefficient trends of reference Cu and of the Cu-XWS_2 composites from wear tests; (b)details on the friction coefficients of the Cu-XWS_2 composites.

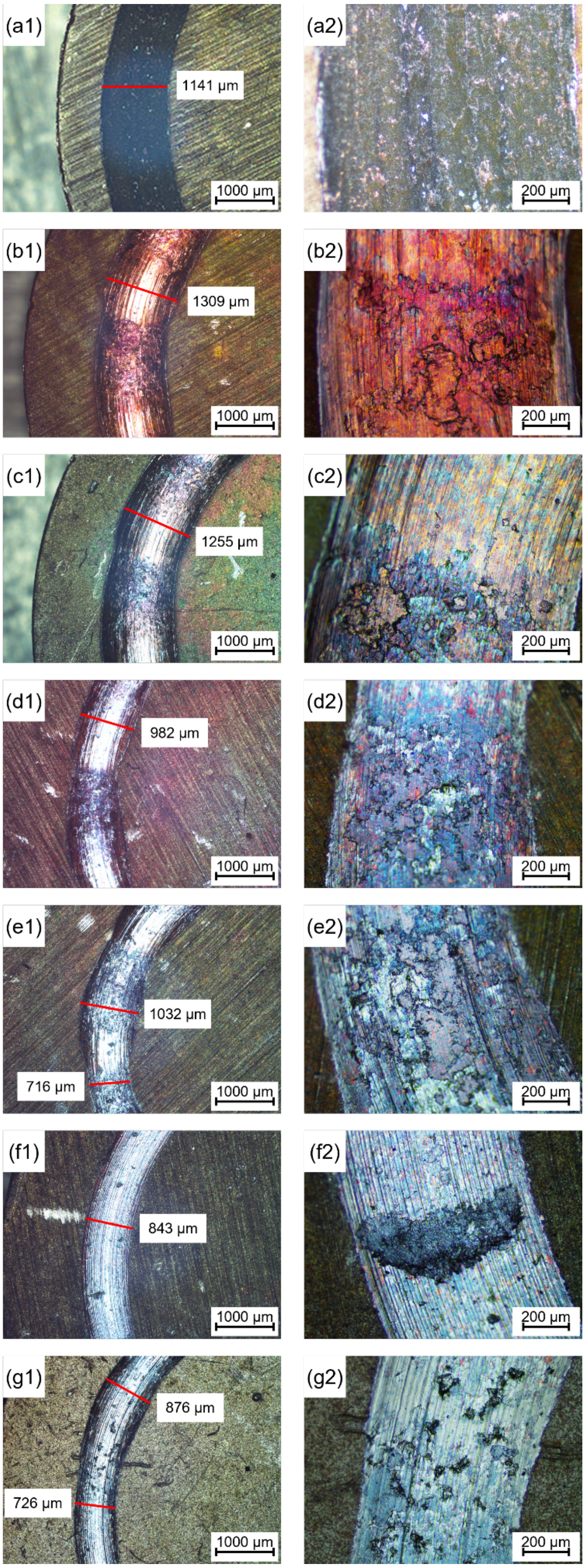

Fig. 17 OM images of the wear tracks of reference Cu and of the Cu-XWS_2 composites: Cu at 25x (a1) and 50x (a2), Cu-5WS_2 at 25x (b1) and 50x (b2), Cu-10WS_2 at 25x (c1) and 50x (c2), Cu-15WS_2 at 25x (d1) and 50x (d2), Cu-20WS_2 at 25x (e1) and 50x (e2), Cu-25WS_2 at 25x (f1) and 50x (f2), Cu-30WS_2 at 25x (g1) and 50x (g2).

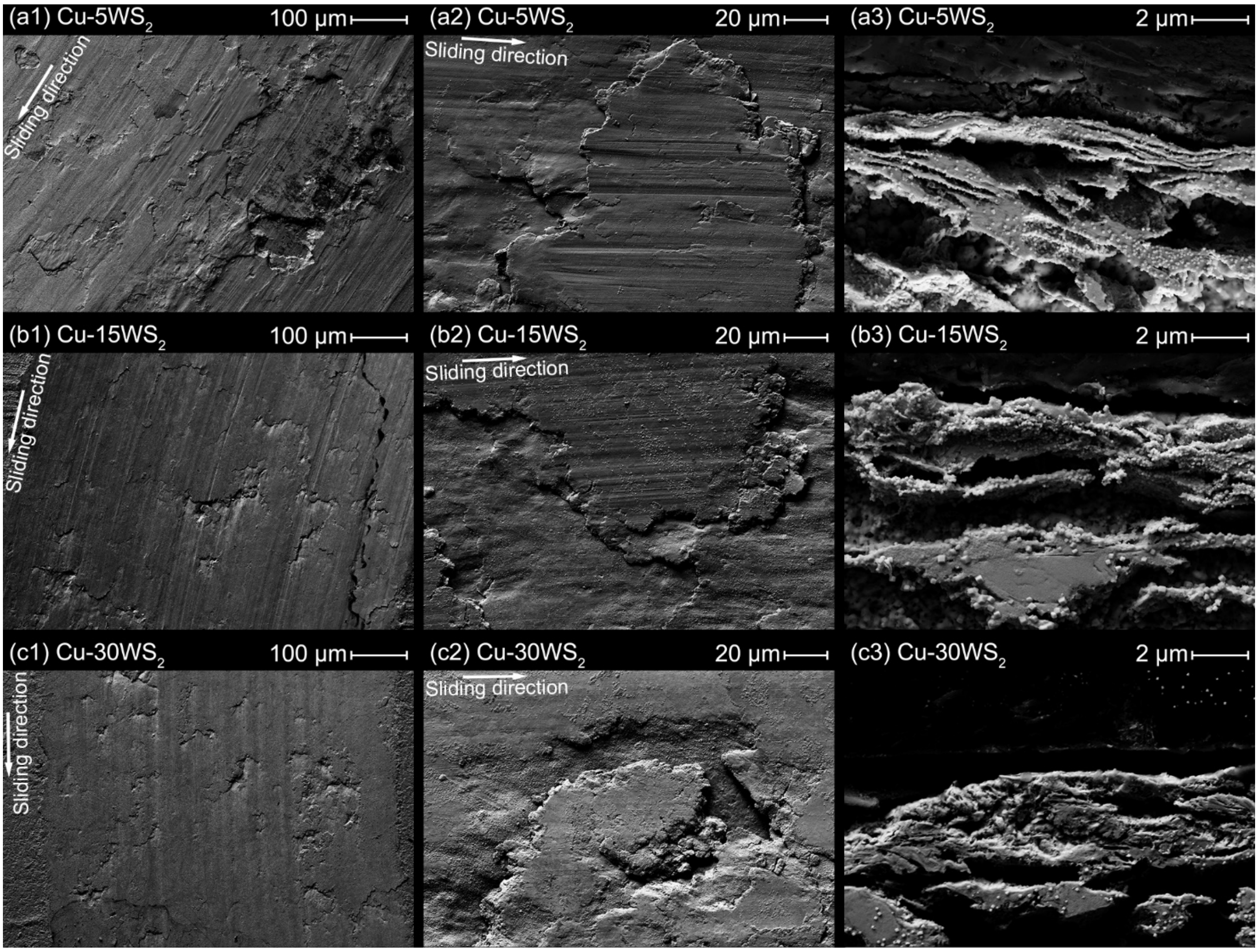

Fig. 18 SEM images of the wear tracks of Cu-XWS_2 composites: Cu-5WS_2 at 400x (a1), 1500x (a2) and cross-section at 20000x (a3), Cu-15WS_2 at 400x (b1), 1500x (b2) and cross-section at 20000x (b3), Cu-30WS_2 at 400x (c1), 1500x (c2) and cross-section at 20000x (c3).

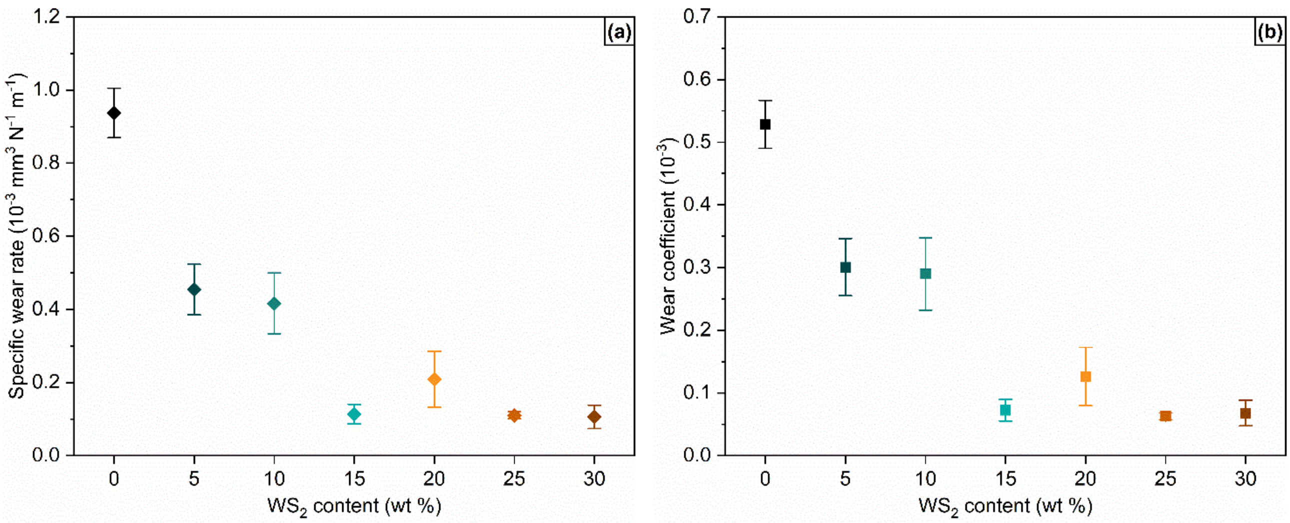

Fig. 19 (a) Specific wear rates and (b) wear coefficients of reference Cu and of the Cu-XWS_2 composites extrapolated from wear tests.